USING DIFFERENTIAL SHEAR STRAIN MEASUREMENTS TO MONITOR

CROSSTIE SUPPORT CONDITIONS IN RAILROAD TRACKS

by

D. Kody Johnson

A thesis

submitted in partial fulfillment

of the requirements for the degree of

Master of Science in Civil Engineering

Boise State University

December 2021

BOISE STATE UNIVERSITY GRADUATE COLLEGE

DEFENSE COMMITTEE AND FINAL READING APPROVALS

of the thesis submitted by

D. Kody Johnson

Thesis Title: Using Differential Shear Strain Measurements to Monitor Crosstie Support Conditions in Railroad Tracks

Date of Final Oral Examination: 01 November 2019

The following individuals read and discussed the thesis submitted by student D. Kody Johnson, and they evaluated the student's presentation and response to questions during the final oral examination. They found that the student passed the final oral examination.

Debakanta Mishra, Ph.D.   Chair, Supervisory Committee

Bhaskar Chittoori, Ph.D.   Member, Supervisory Committee

Ted Sussmann, Ph.D.   Member, Supervisory Committee

The final reading approval of the thesis was granted by Debakanta Mishra, Ph.D., Chair of the Supervisory Committee. The thesis was approved by the Graduate College.

ACKNOWLEDGMENTS

I owe my deepest gratitude to my Advisor and friend, Dr. Deb Mishra, who exhibited remarkable patience and fortitude in working with me throughout my undergraduate and graduate studies and who was integral to my academic success. I would also like to offer special thanks to my friend and colleague, MD. Fazle Rabbi. Our collaboration, discussions and disagreements advanced my understanding immeasurably throughout my graduate career.

ABSTRACT

This thesis details a comprehensive numerical analysis of load determination, and crosstie support assessment and monitoring using strain gauges to measure differential rail shear strain in ballasted railroad tracks due to applied railcar wheel loads. These differential shear strain measurements can be related to applied wheel loading and crosstie support reactions through the geometric and constitutive properties of a given rail section. The basic theory behind the measurement technique was reviewed and investigated using finite element models of varying complexity. The impact of field conditions such as differential ballast and subgrade support, track stiffness, crosstie spacing, gauge installation location, and circuit calibration methods were explored, as well as the nature of the interaction between vertical and lateral loads on accurate load determination. The results of this theoretical study indicate that differential shear strain measurements are a robust method for load and crosstie support assessment and monitoring and can be used for accurate measurement of both vertical and lateral loads.

TABLE OF CONTENTS

LIST OF TABLES

LIST OF FIGURES

LIST OF PICTURES

LIST OF ABBREVIATIONS

1-D	One Dimensional
2-D	Two Dimensional
3-D	Three Dimensional
AREMA	American Railway Engineering and Maintenance-of-Way Association.
cm	Centimeter
D	Distance
E	Modulus of elasticity
FE	Finite Element
FEM	Finite Element Method
GPa	Gigapascal
in.	Inch
kN	Kilonewton
L/V	Lateral to Vertical load ratio
m	Meter
mm	Millimeter
MPa	Megapascal
N/A	Neutral Axis
SVM	Support Vector Machines
US	United States

WILD   Wheel Impact Load Detector

CHAPTER ONE: INTRODUCTION

Wayside measurement of bending-induced shear strains in railway rails is a practice that has been used since the 1970's in various research efforts studying the mechanical behavior of ballasted railway tracks under static and dynamic loading (Ahlbeck et al., 1976; Milkovic´ et al., 2013; Borinder, 2014; Tutumluer et al., 2015; Mishra et al., 2015; Cortis et al., 2017, etc.). A specific application of this practice is in the estimation of wheel loads and the corresponding support conditions of underlying crossties. The basic theory for estimating wheel loads and support conditions is based, in its simplest form, on Bernoulli-Euler beam theory and uses the principle of constant shear between the applied wheel load and the associated supports. Two circuits are typically used: one in the crib section of the rail (the unsupported rail section between two crossties), and one surrounding a crosstie. Each circuit is typically comprised of four dual-element shear strain gauges. Two gauges (one on each side of the rail) are placed at a distance of approximately ten inches from another set of two gauges, with both sets of gauges centered on the crib or crosstie respectively as shown in Figure 1.1. These gauges are used to measure shear strains on either side of the wheel load as it moves through the circuit location. A vertical force balance relates the wheel load or support reaction to shear force. Based on the relationship between shear force and shear strain, measured shear strains can be related to applied wheel loads and support reactions.

Strain gauges mounted at ± 45°
from the longitudinal axis of the
rail on the rail foot

Vertical load
shear gauge

Neutral axis

Lateral load
shear gauge

Strain gauges mounted
at ± 45° from the
neutral axis on the rail
web

Crib shear
Circuit ($\Delta\gamma_c$)

Crosstie shear
circuit ($\Delta\gamma_x$)
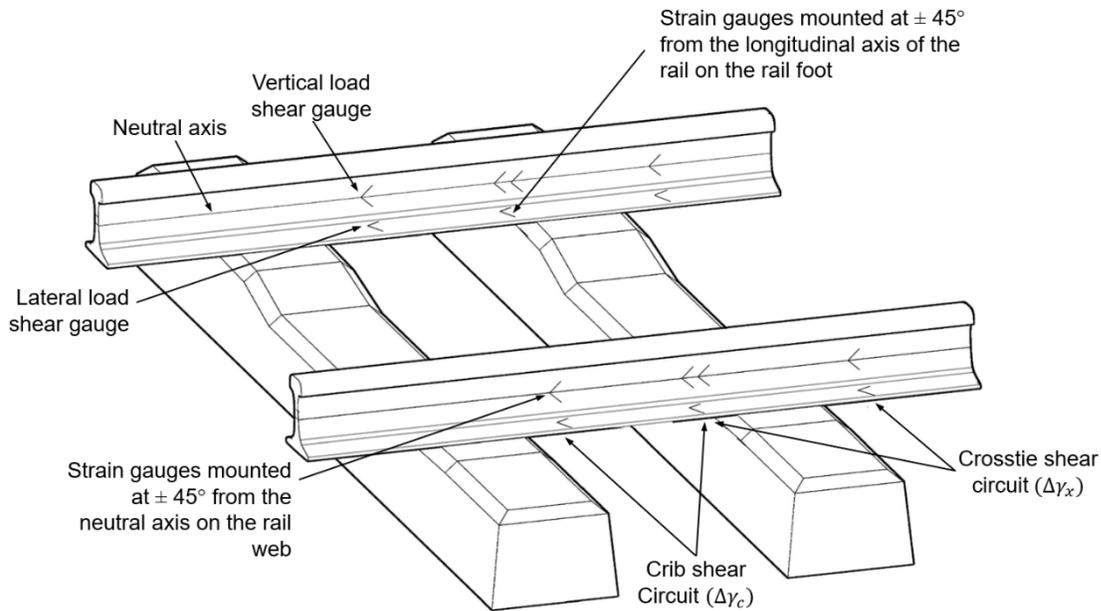
Figure 1.1   Typical Crib/Crosstie Circuit Configuration

While this method has been shown to be very effective in practice by Ahlbeck et al. (1976) and many others over the years, the theoretical validity of applying one-dimensional (1-D) beam theory to the complex three-dimensional (3-D) geometry, material mechanical properties, and boundary conditions that exist in the field has yet to be explicitly verified for determining and monitoring crosstie support conditions over time. Small differences in shear strain measurements can lead to large errors in estimated loads, especially for reaction support conditions. To determine the validity, on a theoretical basis, of using wayside strain gauge measurements to determine rail support conditions and how they change over time, this paper presents a number of static finite element analyses of simplified railway geometries using typical material mechanical properties to quantify the accuracy of these measurements; and how changes in track conditions can magnify any inherent errors in the monitoring method.

Previous Investigations

One of the earliest applications of wayside strain gauge measurements to determine rail loading conditions was proposed by Ahlbeck et al. (1976) drawing on the prior work of Peterson et al. (1971) and Kudryavtsev et al. (1973). The method for measuring vertical wheel/rail forces proposed included the use of eight strain gauges. Two strain gauges (separated by an angle of 90°) were placed at the neutral axis of the rail section oriented at 45° from the longitudinal axis of the rail. Two more strain gauges were similarly placed on the opposite side of the rail. Another set of strain gauges was placed a distance of ten inches from the first set with both sets centered on a crib section of the track as shown in Figure 1.1. As the difference in shear strain between both ends of the circuit are proportional to any applied load between them, an estimate of wheel load was made using a calibration curve created by applying known loads and measuring induced shear strains.

A similar approach was used to determine lateral wheel loads. However, for lateral loads, strain gauges were placed on the foot of the rail section. Unlike for vertical loading, the neutral axis of the rail due to lateral bending passes through the top and bottom of the rail. Consequently, strain gauges cannot be placed at the neutral axis under lateral bending and are thus placed at the rail foot. Strain gauges placed in this location are influenced by the interaction or 'crosstalk' between vertical and lateral loads. To mitigate errors induced by this influence, the gauge output (for both vertical and lateral load circuits) was arranged in a full Wheatstone bridge circuit configuration. This configuration eliminated crosstalk between vertical and lateral loads by separating vertical load-induced strains from lateral load-induced strains and consequently provided robust vertical and lateral load measurements.

Borinder (2014) compared strain gauge measurements of wheel/rail forces to multi-body simulation software results. Generally, the vertical wheel loads calculated from strain gauge measurements were in close agreement with the wheel loads generated using the multi-body simulation software. Lateral forces showed slightly higher deviations between measured values and simulated values, but with a few exceptions were in reasonable agreement.

Cortis et al. (2017) conducted an analysis of lateral rail forces using finite element methods. The model results correlated well with field data and were additionally validated with a small-scale bench study. A method was proposed for determining lateral forces based on a constant support stiffness relating measured web bending strains to lateral force, and the results of the finite element analysis and experimental data were in close agreement.

Tutumluer et al. (2015), and Mishra et al. (2015), conducted an in-depth investigation of the effects of bridge transitions on railbed mechanical behavior. As part of that investigation, strain gauge circuits similar to those proposed by Ahlbeck et al. (1976) were installed in open-track locations, and at near-bridge locations. To monitor changes in crosstie support conditions, an additional circuit was added. This circuit was centered over a crosstie in which support conditions were to be monitored. The circuit was used to measure the crosstie reaction by finding the difference between the applied load determined in the crib circuit and the applied load determined in the crosstie circuit. The percentage of wheel load supported by the crosstie was thus determined from the difference between the crib circuit output and crosstie circuit output. Based on a common assumption that a loaded crosstie carries approximately 40% of the wheel load for a well-maintained track, the measured difference in output between the two circuits should correspond to an

approximate load of 40%. The measurements recorded in this study were consistent with this assumption and by using this technique the researchers were able to monitor changes in support conditions over time. It was generally found that for well supported crossties (no crosstie/ballast gaps), the percentage of load carried by the crosstie near the bridge transitions exhibited much more variation than open track locations consistent with the complex dynamic behavior expected near bridge transitions resulting in load amplification.

Purpose

As previously mentioned, the investigation by Tutumluer et al. (2015) used the difference between the crib circuit and crosstie circuit outputs to determine the crosstie reaction. The magnitude of this reaction was then used to assess the relative stiffness of the support provided by the underlying ballast and subgrade, and to monitor changes in track conditions over time. While this method was a simple extension of long-established techniques for monitoring wheel loads, there were concerns raised in the industry regarding the validity of the method. One of the primary concerns was in the determination of the crosstie reaction. Direct measurement (using a load-cell) of the crosstie reaction was not carried out. Instead, and as previously discussed, the difference between the crosstie and crib circuits was used and it was uncertain how track conditions impacted the validity of this technique. While the technique provides a time-history of the relative degradation of support on an instrumented crosstie, an understanding of the percentage of wheel load caried by an instrumented crosstie over a wide range of varying track conditions is required to accurately determine crosstie reaction magnitude without direct load-cell measurements (considered impractical for routine use by field practitioners). Additionally, without the use of load-cell measurements, it wasn't possible to directly determine the calibration curve

of the crosstie circuit. Instead, the calibration curve of the adjacent crib circuit was used as an estimate of the load/strain response of the crosstie circuit. However, the different loading conditions between the two circuits and corresponding differences in deflected shape may introduce errors in load/strain response and thereby introduce errors in crosstie reaction measurements.

With these considerations in mind, the purpose of this research effort was to investigate:

1. the theoretical validity of using differential shear strain theory to measure vertical and lateral loads and crosstie support conditions under the complex 3-D strain environment of the rail under various loading and support conditions;

2. the nature of the interactions between vertical and lateral loads and their impact on load determination and crosstie support monitoring;

3. the application of the crib circuit load/strain response (calibration curve) to estimate the load/strain response of the crosstie circuit and the accurate determination of crosstie reaction magnitudes.

Scope

This investigation is divided into three main sections. The first two sections, Chapter 2 and Chapter 3, each consist of a published manuscript. The first manuscript, *Effect of Track Configuration and Loading Conditions on Vertical Wheel Load Measurements Using the Differential Shear Approach,* was published in the Transportation Research Record: Journal of the Transportation Research Board in 2019. This manuscript explores the differential shear strain theory beginning from a simple 1-D Bernoulli-Euler beam analysis and progresses through several finite element analyses of a full-track model

based on typical parameters of ballast strength, subgrade strength, etc. The shear strain distribution on the face of the rail web of a simply supported rail section under load was plotted and used to determine the ideal strain gauge installation location for accurate vertical load measurements. Additionally, the impact of support conditions such as crosstie spacing, ballast stiffness, and weakly supported crossties were explored. Finally, calibration procedures and techniques were investigated to assess the impact of calibration methods on the accuracy of calibration curves and associated wheel load measurements.

The second manuscript (Chapter 3), *Quantification of Vertical and Lateral Loads Using Strain Gauges—Eliminating the Wheatstone Bridge,* was published in the Proceedings of the 2019 ASME Joint Rail Conference. This investigation explores the nature of the interactions between vertical and lateral load using a simply supported finite element rail section. Because field measurements using the full Wheatstone bridge mask the interactions between vertical and lateral loads internally and only output a single shear value, the circuit behavior of the Wheatstone bridge was eliminated. Instead, virtual strain gauges were modeled by calculating strains based on nodal deformations at the surface of the rail web. The precise relationship between vertical/lateral load-induced strains and applied loading was then established using a linear regression analysis. It was demonstrated that vertical/lateral load interactions have no impact on vertical load determination, but that these interactions do have a significant impact on lateral load determination.

Chapter 4 consists of an investigation of the validity of applying the load/strain response (calibration curve) of the crib circuit to the crosstie circuit in determining crosstie reaction magnitude. A revised full-track finite element model was developed to incorporate certain model refinements over previous models. The crosstie geometry used in previous

analyses was revised to be more representative of existing crosstie geometry used in high-speed rail applications. Frictional contacts, as opposed to tied constraints, were added between the rail and rail pad to allow the rail to slip and or deflect away from the rail pad under loading. Two additional crossties were added to the model to increase the total number of crossties from seven to nine. This change was made to minimize boundary effects caused by reactions at the outermost crossties in the model. The revised model was then loaded with varying vertical load magnitudes, and a regression analysis was conducted to determine load/strain response of the crib circuit. Subsequently, the crosstie circuit was loaded, and the load/strain relationship determined from the crib circuit was used to determine the load magnitude. Close agreement between the applied load and calculated load indicates that vertical crosstie reactions can be accurately calculated by applying the crib circuit calibration curve to the crosstie circuit.

CHAPTER TWO: MANUSCRIPT ONE — EFFECT OF TRACK CONFIGURATION AND LOADING CONDITIONS ON VERTICAL WHEEL LOAD MEASUREMENTS USING THE DIFFERENTIAL SHEAR APPROACH

Abstract

Measurement of vertical wheel loads on railroad tracks using strain gauges mounted on the rail web is common practice. This measurement approach makes use of the differential shear concept: "the difference in shear force between two points along a beam equals the magnitude of the vertical load applied between those two locations". Although the applicability of this concept is easy to verify for simple beams, its validity for field applications under different track configurations including support and loading conditions is relatively unexplored. This manuscript presents findings from an ongoing research effort that has utilized numerical models to assess the effects of different track and loading configurations on vertical wheel load measurements using the differential shear approach. The underlying theory behind this measurement approach is first introduced, and different scenarios are compared using a simple 1-D model. This is followed by detailed analysis of the effects of different vertical, lateral, and axial loading combinations on the measured shear strain values. Finally, a 3-D Finite Element Model is used to study the dependence of the measured wheel loads and calibration approaches on track support conditions. Findings from the analyses clearly establish the applicability of this measurement approach across different scenarios observed in railroad tracks.

Introduction

One of the most common wayside instrumentation techniques employed for the determination of vertical railcar wheel loads is the placement of strain gauges on the rail web to measure differential shear strain. The basic theory behind this method was first presented by Ahlbeck et al. (1976) and is based on a simple principle: the difference in vertical shear force between two locations along a beam is equal to the magnitude of the vertical load applied between those locations. Reasonably accurate estimates of wheel load magnitude can be obtained by measuring the differential shear strain between two locations using strain gauges and relating those measurements to the vertical shear force (and thereby vertical loading) through rail geometric and constitutive properties. This basic technique forms the backbone of the Wheel Impact Load Detector (WILD), one of the most widely used wayside monitoring systems by the railroad industry.

One common method of measuring differential shear in the field is by mounting strain gauges at the neutral axis of the rail. From mechanics, the principal strains under a vertical-only loading configuration are oriented at 45 degrees to the neutral axis of a beam. Accordingly, measuring the strain at an angle of 45 degrees to the neutral axis will help establish the magnitudes of the principal strains, which can then be resolved to get the shear strain values. Although this measurement approach is valid in 2-D, the effects of different field conditions (in terms of track structure, loading, and support conditions) on strain gauge measurements are still unknown. For example, the rail is often subjected to significant longitudinal and lateral loads that result in strains in multiple directions; moreover, bending stresses in the web as well as out of plane shear strains lead to strain fields that cannot be simplified using "vertical-only" assumptions. Finally, variation in rail

section properties, the vertical location of the strain gauges in the rail web, the horizontal distance from the face of adjacent crossties, and crosstie support conditions are all factors that may significantly impact strain measurements in the field. During field instrumentation applications, these strain gauge circuits, which are usually installed in a Wheatstone bridge configuration, are calibrated under typical loading and support conditions. Nevertheless, how these calibration results are affected by changing field conditions and complex loading conditions has not been thoroughly investigated.

A recent study at Boise State University in the US focused on investigating the effects of different calibration procedures, installation locations, support conditions, and track configurations on the shear strain values measured using the differential shear approach. Extensive numerical modeling was carried out using the Finite Element Method (FEM) to simulate the strain-based load measurement approach in the field. The effects of different load and support conditions were studied, and their effects on the magnitudes of the backcalculated loads were quantified. This manuscript presents initial findings from this research effort. Results pertaining to the effects of localized soft spots in the track substructure and how this theory can be extended to evaluate the support conditions underneath crossties will be presented in subsequent manuscripts.

Research Objective and Scope

The primary objective of this research effort was to evaluate how strain gauge placement and calibration, various track configurations, and support and loading conditions can affect the accuracy of vertical loads backcalculated using the differential shear approach. First, a simple 1-D model of a beam supported at multiple locations was analyzed under different loading conditions to link the differential shear magnitudes to the applied

load levels. This was followed by FE analysis of a 3-D track structure incorporating typical rail and tie geometries. This 3-D model was analyzed under different tie spacing, rail sections, and support conditions to assess the impact that these factors have on the accuracy of differential shear measurements and backcalculated load magnitudes.

Basic Theory

As already mentioned, the concept of the difference in shear force at two points along a beam being equal in magnitude to the load applied between is easy to verify under simply supported or similar statically determinate structural configurations. However, a rail is supported at multiple points by crossties (which can be idealized as elastic supports), and therefore represents an indeterminate structural configuration. The first task in this research effort was to use a simple 1-D model to analyze a simplified rail segment supported by multiple elastic springs. Apart from calculating the shear force magnitudes under different support conditions, this task also involved studying the effects of variations in support spacing on the induced shear forces. Results from this analysis are presented in Figure 2.1.

Figures 2.1.a and 2.1.b comprise crossties that are assumed to be fixed in the vertical direction (no vertical deflection), whereas the crossties in Figures 2.1.c and 2.1.d are supported by springs with a stiffness of 250 kN/mm. Note that this spring stiffness value is similar to that reported by Mishra et al. (2015). Figures 2.1.b and 2.1.d represent cases where crosstie # 6 was removed to study the impact of variable support spacing and unsymmetrical loading conditions. Note that the 1-D beam analysis assumes Euler-Bernoulli beam behavior. For rigid supports with typical crosstie spacing, this assumption is not valid due to the depth to length ratio of the rail within the crib. However, due to the

a) 11 Vertically Non-Deformable Crossties

b) 10 Vertically Non-Deformable Crossties
(Tie #6 Removed)

c) 11 Crossties on Spring Support
(k = 250 kN/mm)

d) 10 Crossties on Spring Support
(Tie #6 Removed, k = 250 kN/mm)
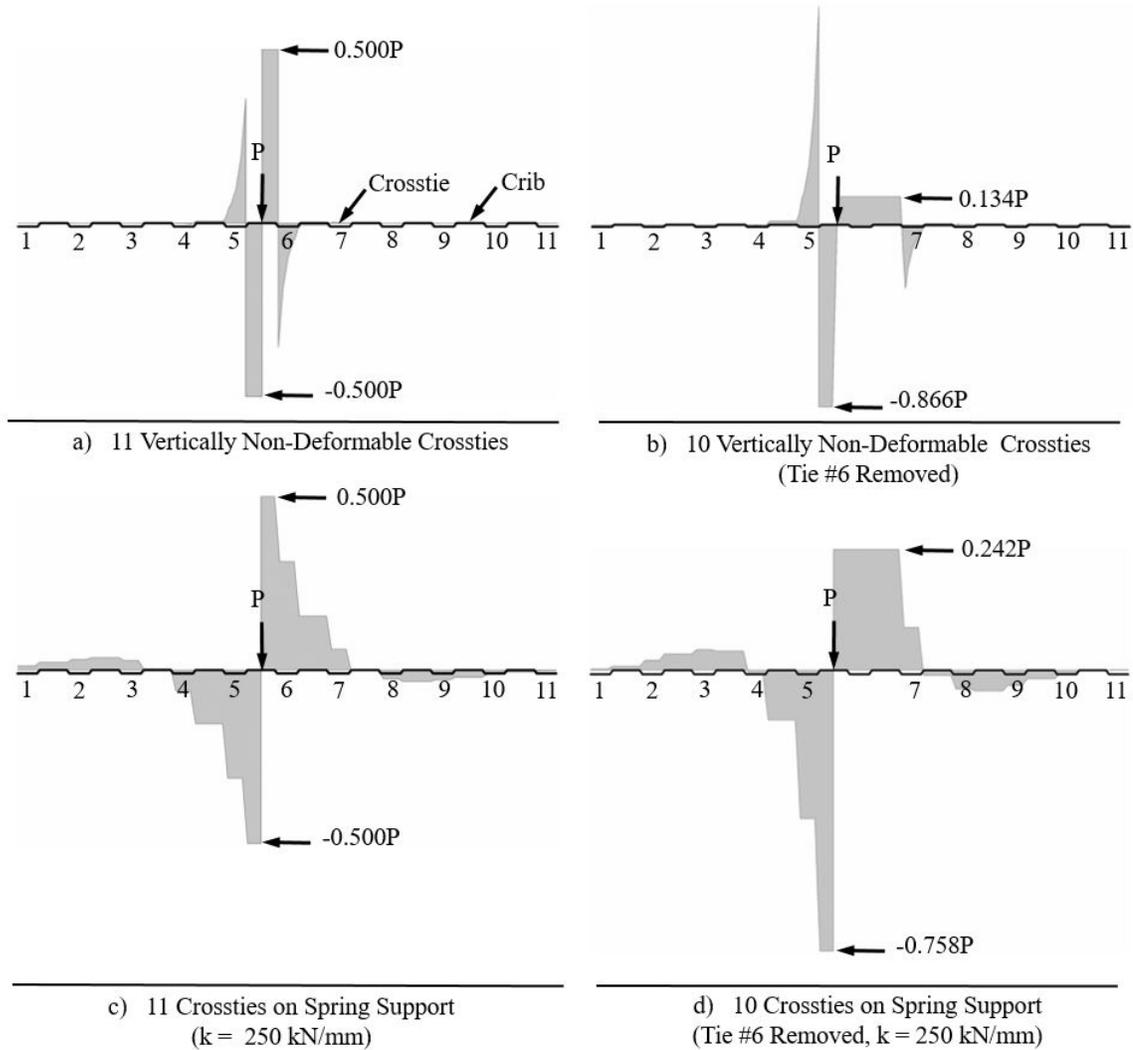
Figure 2.1   1-D Shear Analysis of Continuous Beam on Multiple Supports

relatively high deflection that occurs at the supports, the impact of this assumption on the associated shear analysis is negligible.

As seen from Figure 2.1, the difference in shear force on either side of the load P is always equal to P regardless of span length, the number of supports, or support conditions (rigid vs. deformable). Therefore, knowledge of the magnitude of the shear force on either side of an applied load is sufficient to determine the load magnitude. Although the actual magnitude of the shear force changes based on the support conditions, the difference between the values on either side of the load remains unchanged. With the validity of the

differential shear approach across different support spacing and support types established, the next step involved in-depth study of the strain measurement approach in the field.

Figure 2.2 shows the schematic layout of a typical strain gauge configuration on the rail web, and the idealized 2-D strain states associated with an applied vertical wheel load P. Only one face of the rail web is shown in Figure 2.2. In practice, a total of eight strain measurements are performed with 4 dual-element strain gauges: two on each face.
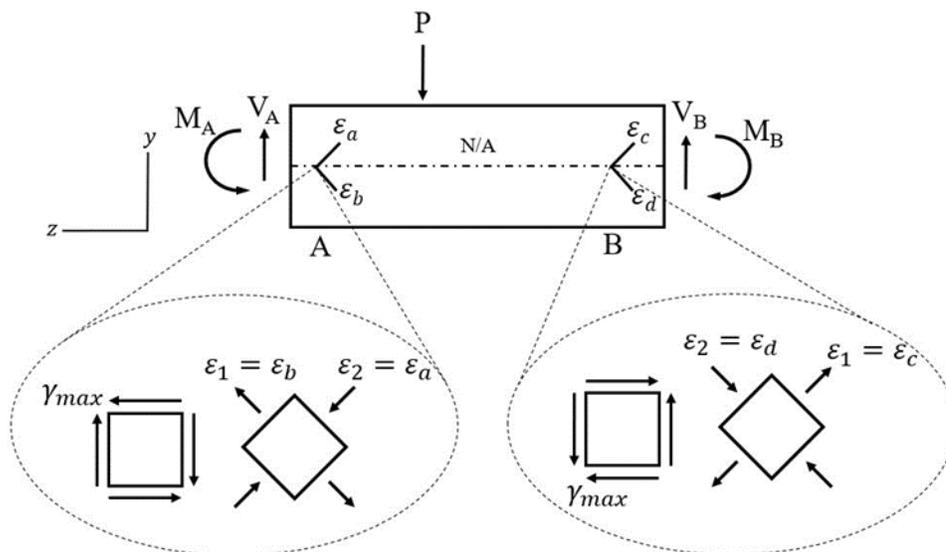
Figure 2.2   Strain Gauge Orientation and Rail Web Strain State

With the proper configuration of the gauges into a Wheatstone bridge circuit, an average of the strain measured on both faces of the rail web is used to calculate the differential shear. By orienting the strain gauges at an angle of 45 degrees from the rail longitudinal axis, the measured strains due to the load correspond to the principal strains in the plane of the web.

The magnitude of P is proportional to the change in the maximum shear strain between points A and B (Figure 2.2) according to the following relationships:

$$\gamma_{max} = \varepsilon_1 - \varepsilon_2 \qquad (2.1)$$

$$V = \frac{\gamma E I t}{2Q(1+v)} \qquad (2.2)$$

$$P = V_A - V_B = \frac{E I t}{2Q(1+v)}(\gamma_A - \gamma_B) = \frac{E I t}{2Q(1+v)}[(\varepsilon_1 - \varepsilon_2)_A + (\varepsilon_1 - \varepsilon_2)_B] \qquad (2.3)$$

where

V = vertical shear force;

γ = maximum shear strain;

E = modulus of elasticity;

I = moment of inertia of the rail section;

t = web thickness;

Q = statical moment of area of the rail section;

v = Poisson's ratio;

ε = principal strain;

The wheel load determined using this principle (Equation 2.3) in actual field applications is approximate. The true 3-D strain state is more complex than the simplified pure shear state shown in Figure 2.2. Normal and shear stresses from longitudinal and lateral loading can cause a rotation of the principal strain axes and additional out of plane deformations. These factors along with geometric and material property variations make it necessary to calibrate strain gauge circuits under typical load and support conditions. Nevertheless, with proper calibration and placement, accurate and reliable load estimates can be obtained. However, changes in cross sectional properties or large deviations from the initial placement in respect to the neutral axis, for example due to excessive rail wear, may necessitate recalibration.

Impact of Loading Conditions on Vertical Load Estimates

To gain a better understanding of the impact that variations in load and support conditions can have on strain gauge measurements, a virtual FEM experiment was conducted to compare strain gauge deformations with theoretical shear strain values. A simple 3-D FEM model of an AREMA 132RE rail (supported at both ends) was constructed using the commercial software ABAQUS® as shown in Figure 2.3.
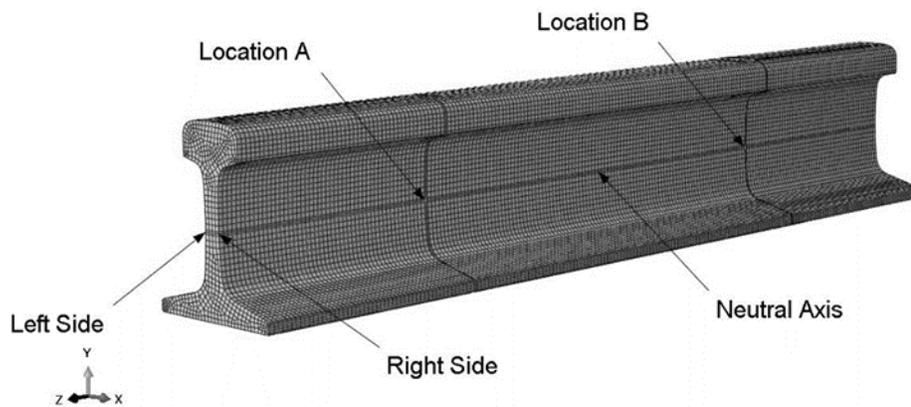
Figure 2.3   FEM Model of AREMA 132RE Rail Section

The model was 1-m long and was centrally loaded with vertical and lateral loads under different support constraints. Virtual strain gauges were placed at the neutral axis of the rail section at the longitudinal quarter points on both faces of the rail web. The virtual strain gauge consisted of a 4 mm x 4 mm square element with a diagonal length (gauge length) of 5.7 mm. The type of element chosen for this model was the ABAQUS® 3D8I element which is a linear hexahedral element with additional internal degrees of freedom to reduce parasitic shear and artificial stiffening due to bending (ABAQUS, 2015). This element performs nearly as well as quadratic elements provided they are rectangular in shape, but at much lower computational costs. The mesh was assigned a global size of 5 mm, and this configuration resulted in nearly cubical elements within the web of the rail.

Two types of calculations were carried out to establish the shear strain magnitudes, and backcalculate the corresponding applied vertical loads. Virtual gauge calculations used nodal deformations to calculate the principal engineering strains, ε_1 and ε_3 along the respective diagonals of the gauge elements. The theoretical calculations directly used the shear strain, ε_{23} , values output from the FEM model. The results of this virtual experiment are summarized in Table 2.1. The gauge calculations show large fluctuations in the predicted load magnitude depending on load and constraint conditions, whereas the theoretical calculations show a relatively constant 0.3-0.5% error in vertical load predictions regardless of loading conditions. One important distinction between the two calculations is that the shear strain reported by ABAQUS (ε_{23}) is the shear only in the y-z plane whereas the shear determined from nodal deformations is dependent on 3-D rail behavior similar to the deformations experienced by a physical strain gauge. Additionally, the rail web is not perfectly vertical at the neutral axis. The deformation recorded by a strain gauge is not strictly in the same plane as the ε_{23} values reported. Furthermore, the strain in the transverse direction is not insignificant and in some circumstances is as large as the normal strains in the vertical and longitudinal directions. This additional out of plane deformation can be another potential source of error in load estimates.

The fluctuation of vertical load estimates obtained from gauge calculations indicates at least some dependence of strain gauge measurements on loading conditions. Note that the gauge calculations listed in Table 2.1 represent what an actual strain gauge will measure in the field, whereas the theoretical values (ε_{23}) represent what the strain values would be if the assumptions inherent in Figure 2.2 were perfectly valid. As seen

from Table 2.1, an axial constraint (restricting axial displacement at both ends of the beam)

creates a minimal

Table 2.1   Comparison of Estimated Loads: Strain Gauge vs. Theoretical

				Gauge (Nodal Coordinate Deformation)				Theoretical (Model ε_{23})			
Loading (kN) and Axial Constraint (Yes, No)				γ ($\mu m/m$) Strain Location		Estimated Load		γ ($\mu m/m$) Strain Location		Estimated Load	
V	A	L	Axial Constraint	A	B	P (kN)	% Diff.	A	B	P (kN)	% Diff.
100	-	-	No	257.1	-257.1	100.7	0.6%	256.5	-256.5	100.4	0.4%
100	-	-	Yes	256.8	-256.8	100.5	0.5%	256.2	-256.2	100.3	0.3%
100	-	10	No	256.2	-253.1	100.3	0.3%	256.6	-256.5	100.4	0.4%
100	-	25	No	251.7	-250.7	98.4	-1.6%	256.5	-256.5	100.4	0.4%
100	-	50	No	235.6	-231.6	91.5	-8.5%	256.5	-256.5	100.4	0.4%
100	-	50	Yes	238.0	-238.0	93.2	-6.8%	256.2	-256.2	100.3	0.3%
100	-	100	No	171.1	-155.2	63.9	-36.1%	256.6	-256.6	100.4	0.5%
100	-	100	Yes	181.6	-181.6	71.1	-28.9%	256.3	-256.3	100.3	0.3%
100	50	-	No	257.1	-257.1	100.7	0.6%	256.5	-256.5	100.4	0.4%
100	50	50	No	235.6	-231.7	91.5	-8.5%	256.6	-256.6	100.4	0.4%
100	50	50	Yes	238.1	-238.1	93.2	-6.8%	256.3	-256.3	100.3	0.3%
100	50	100	No	171.2	-155.2	63.9	-36.1%	256.6	-256.6	100.5	0.5%
100	100	-	No	257.1	-257.7	100.7	0.7%	256.5	-256.5	100.4	0.4%
100	100	-	Yes	256.9	-256.9	100.6	0.6%	256.3	-256.3	100.4	0.3%
100	100	25	No	251.8	-250.8	98.4	-1.6%	256.6	-256.5	100.4	0.4%
100	100	50	No	235.7	-231.7	91.5	-8.5%	256.6	-256.6	100.4	0.4%
100	100	100	No	171.2	-155.3	63.9	-36.1%	256.6	-256.6	100.5	0.5%
100	100	100	Yes	181.7	-181.7	71.1	-28.9%	256.4	-256.4	100.4	0.4%
0	0	100	No	-85.9	-101.9	-36.8	n/a	0.040	-0.049	0.001	n/a

V: Vertical Load

A: Axial Load

L: Lateral Load

Axial Constraint: Longitudinal (axial) displacement constrained at both ends of the rail.

Strain Locations A and B correspond to the locations shown in Figure 2

reduction in the estimated load. Axial load alone appears to have very little effect on strain

gauge measurements. This indicates that the differential strain measurement approach

should yield reasonably accurate values irrespective of the inherent thermal stresses in the

rail. Lateral loads, on the other hand, have a significant impact on the estimated load

magnitudes. In the extreme case, with the lateral load equal to the vertical (L/V=1), the error in vertical load estimates is approximately 28-37%.

Interestingly, in a scenario where only a lateral load of 100 kN magnitude is applied to the rail (no vertical or axial load applied), the estimated load using Equation 2.3 is -36.8 kN (refer to the last row of Table 2.1). This explains why the estimated vertical load is lower by ~30% when L/V=1. As the L/V ratio decreases, the effect of lateral load becomes negligible. The lateral load induced by a 100 kN vertical load on a 1:20 rail cant is approximately 5 kN. Interpolating from Table 2.1, this would result in the estimated load being 0.15% lower than the actual applied load. Similarly, when the load is positioned at the outside rail edge, there is a negligible decrease in estimated load percentage (0.38%). Due to these negligible impacts and to simplify modeling efforts, all subsequent full-track models in this study ignore rail cant and the position of the vertical load on the rail.

In practice, properly placed and calibrated strain gauges on straight sections of track that experience minimal dynamic railcar/trackbed interaction obtain very accurate vertical load estimates. This is supported by the data in Table 2.1. For curved sections of track or for areas with high dynamic railcar/trackbed interaction, measurements of lateral load in conjunction with data similar to the data shown in Table 2.1 could potentially be used to adjust vertical load estimates to correct for the effects of lateral load.

Impacts of Installation, Calibration and Support Conditions on Vertical Load Estimates

A layered elastic, axisymmetric FE model of an AREMA 132RE rail section was developed, as shown in Figure 2.4. The model was developed to gain insight into the impact that various installation locations, calibration procedures, and crosstie support conditions

have on strain gauge measurements. The model comprised a rail on seven crossties modeled with an axisymmetric boundary at the track center.
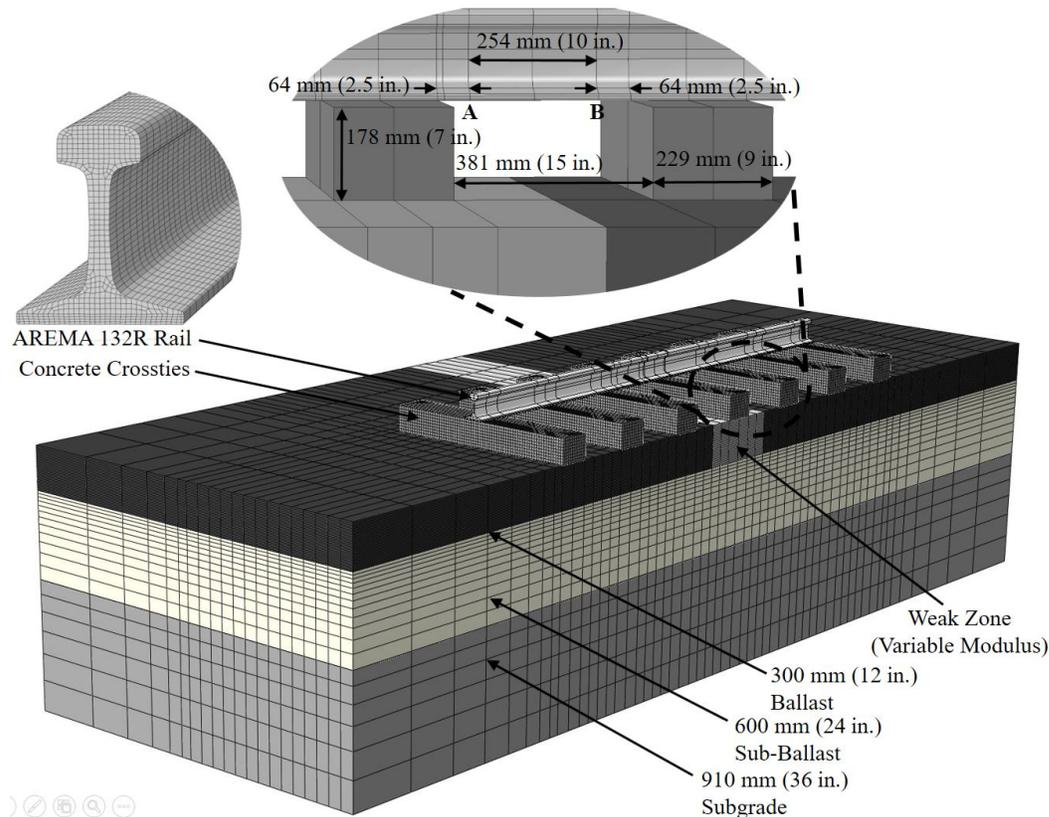
Figure 2.4   FEM Railway Model

A sensitivity analysis was performed to assess the effect of model extent on the values of interest in this study; results from the parametric analysis indicated that a model comprising seven crossties was sufficiently accurate for the purpose of this study. The crossties were placed on a ballast layer with a modulus of elasticity (E) of 230 MPa overlying a sub-ballast layer (E = 140 MPa) which in turn was placed on top of a subgrade layer (E = 70 MPa).

The crossties were placed at 610 mm (24 in.) center-to-center, and were modeled as concrete, with an elastic modulus value of 20.7 GPa. A zone of variable modulus was introduced to study the impact that weakly supported or hanging crossties may have on

vertical load estimates. The initial gauge installation locations (A and B in Figure 2.4) were taken from the configuration used by Mishra et al. (2015).

For vehicle speeds below the critical track velocity and assuming minimal dynamic railcar/railbed interaction, static and dynamic track behavior is comparable; a static FE analysis can therefore provide reasonably accurate results (Kouroussis, 2015; Feng, 2011). These underlying assumptions were key in choosing only static or quasi-static simulations for this research effort. Though ignoring dynamic effects, a static analysis can provide an understanding of some of the key parameters affecting strain gauge measurements.

A biased meshing scheme was used to provide increased nodal densities in areas of interest while reducing computational effort in other areas. Care was taken to ensure the mesh for all parts (layers, rail, and crossties) shared nodes at all interaction boundaries to aid in mesh convergence and help decrease runtimes. The model was meshed with C3D8R elements for their low computational requirements (ABAQUS, 2015). While this linearly interpolated element may not be the most accurate element available, the reduction in computational effort compared to other element types was desirable.

Installation

One of the implications of Figure 2.1 is that the shear force instantly changes direction from one side of the applied load to the other. However, actual instrumentation data obtained in the field shows there is a 'shoulder' on either side of an applied load in which the shear more gradually changes direction and achieves its maximum value. This is true for both the applied load as well as the crosstie reactions. For accurate vertical load estimates, the strain gauges must be placed outside the impact zone of these boundary effects. To gain insight into the relative size of these boundary areas, and thereby determine

the ideal gauge installation locations, the percent estimated load was calculated from shear

strain values taken symmetrically on both sides of the crib center. The results have been

plotted in Figure 2.5.
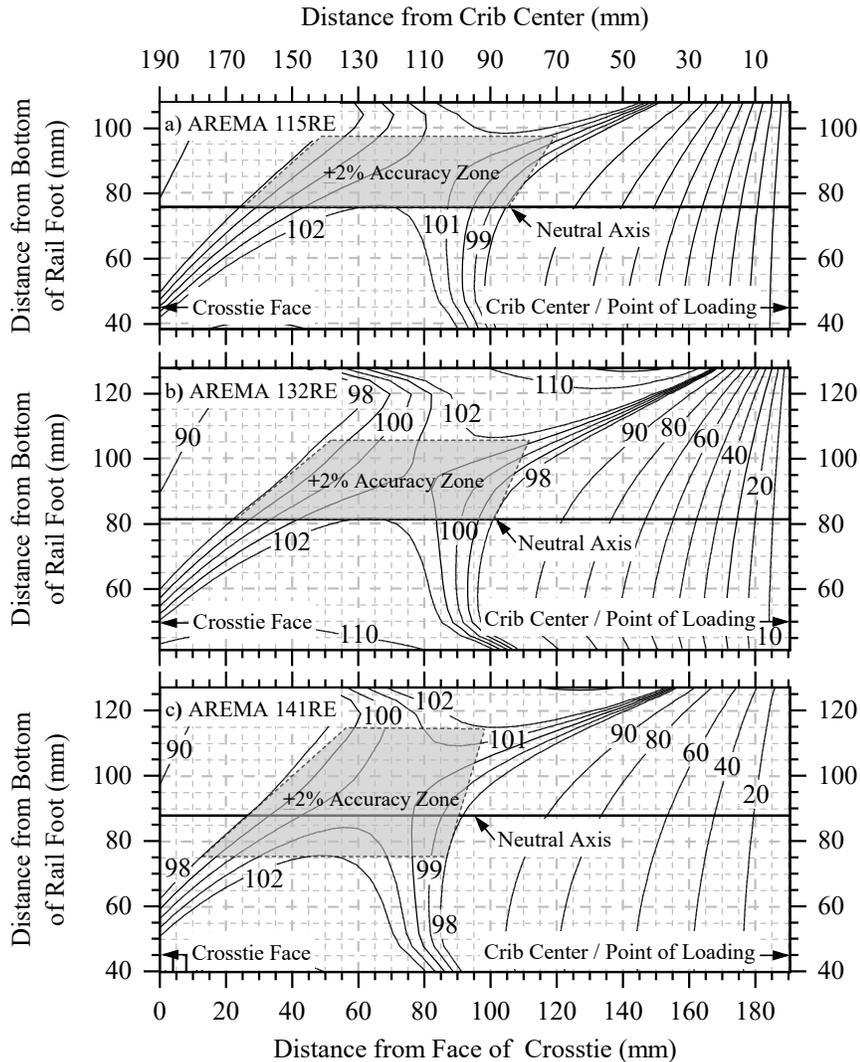
Figure 2.5   Variation in Estimated Vertical Load (Expressed as a Percent of Applied Load) with Strain Gauge Position along the Rail for (a) 115 RE, (b) 132 RE, and (c) 141 RE Rail Sections

The contours represent the estimated load (calculated by finding the difference

between the shear strain at a given location and its symmetric pair on the opposite side of

the crib center) as a percentage of the applied load. The contours show significant impacts

from the load and sleeper boundary areas resulting in a reduced area where strain gauge installation would lead to accurate load estimates. The largest boundary effect is due to the load as the shear at the point of loading is zero. This results in a shift in the optimal placement location away from crib center toward the crossties. The boundary effect caused by the crossties is much less significant resulting in ~10% reduction of accuracy at the crosstie face.
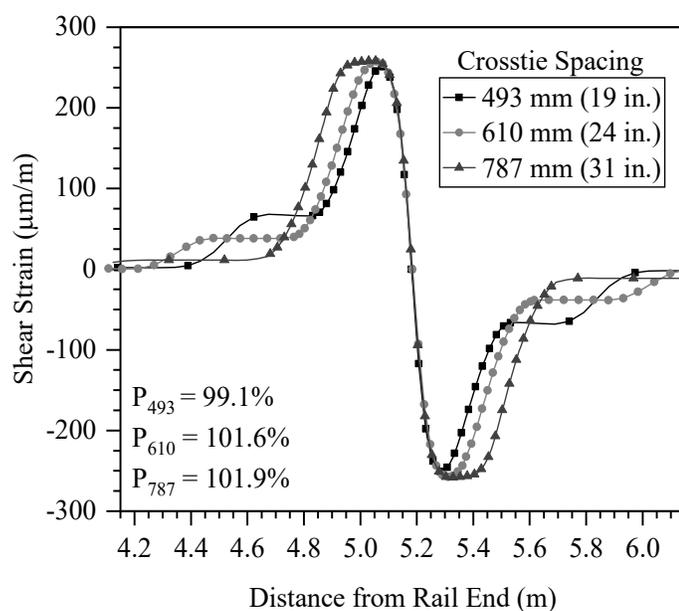
Figure 2.6   Impact of Crosstie Spacing (Center to Center) on Vertical Load Estimates

For the 610 mm (24 in.) center-to-center crosstie spacing used in this study, the shear distribution reaches a maximum value within a relatively small region indicating it may be difficult to achieve the same accuracy with shorter crosstie spacing. To investigate the impact of crosstie spacing on strain gauge measurements, crossties placed at distances of 493 mm (19 in.) and 787 mm (31 in.) center-to-center were also modeled; a comparative plot has been presented in Figure 2.6. With longer crosstie spacing, the region of maximum shear strain increases in length toward the crosstie face providing more leeway in gauge

placement. Conversely, reducing the spacing from 610 mm (24 in.) to 493 mm (19 in.), resulted in a slight decrease (2.5%) in the accuracy of the estimated percent load. Based on these results, for crosstie spacing significantly less than 493 mm (19 in.), estimation of the applied load levels using the differential shear concept may be difficult due to boundary effects.

The optimal strain gauge installation location for a 610-mm (24-in.) crosstie spacing is summarized in Table 2.2. Note that the values listed in the table are approximate, as mesh size, element type, and model extent can all impact the accuracy of the analysis. In addition, the actual contact area between the rail and the rail pad/seat are not considered. The contact area of the rail seat is slightly less than the thickness of the crosstie, so values from Table 2.2 should be adjusted to reflect the actual contact area between the rail and the rail pad.

Table 2.2   Optimal Strain Gauge Installation Locations

	Horizontal Distance in mm (in.)	
Rail Section	From Crosstie	From Crib Center
115RE	65 (2.6)	126 (4.9)
132RE	62 (2.4)	129 (5.1)
141RE	59 (2.3)	132 (5.2)

By placing the gauges near the locations listed in Table 2.2, initial uncalibrated circuits will measure loads as accurately as possible. This increases the stability of the measurements with changing conditions and reduces the 'shift' achieved through calibration. For example, in a scenario where the rail moves longitudinally ('running rail' scenario), finding the optimal strain gauge placement would likely increase the installation life as it would take longer for the gauge to move into an area significantly impacted by boundary effects.

Calibration

The next step in this study involved studying the effects of different calibration approaches on strain gauge measurements. The most common method used to calibrate the differential shear strain gauge circuit involves the use of a hydraulic jack to incrementally apply a known load and measure the induced strain. Typically, the hydraulic jack is constructed in the center of an A-frame that is attached to the rail head on both sides of the jack as shown in Picture 2.1

Picture 2.1   Typical Calibration Apparatus & Procedure

A load cell attached to the jack monitors the applied load as the jack applies a vertical load to the top of the rail. In addition to the measured downward vertical force, the A-frame applies a compressive axial force and a vertical uplift force on the rail. It is these forces and the changes in the relative magnitude of these forces with the size of the A-frame used to calibrate the circuit that have led to discussions on the impact of various calibration configurations. To investigate these potential impacts, four A-frame configurations were simulated in the FEM model shown in Figure 2.4: a 122-cm (48-in.) short span A-frame, a 183-cm (72-in.), medium span A-frame, a 244-cm (96-in.) long span A-frame, and a control case with no frame (vertical loading only). The results from this analysis are presented in Figure 2.7.

Clearly, the shear strain distribution along the neutral axis of the rail varies depending on the A-frame used to apply the load. However, all four shear strain curves converge within the crib. This indicates that the load estimated from the strain gauge circuit
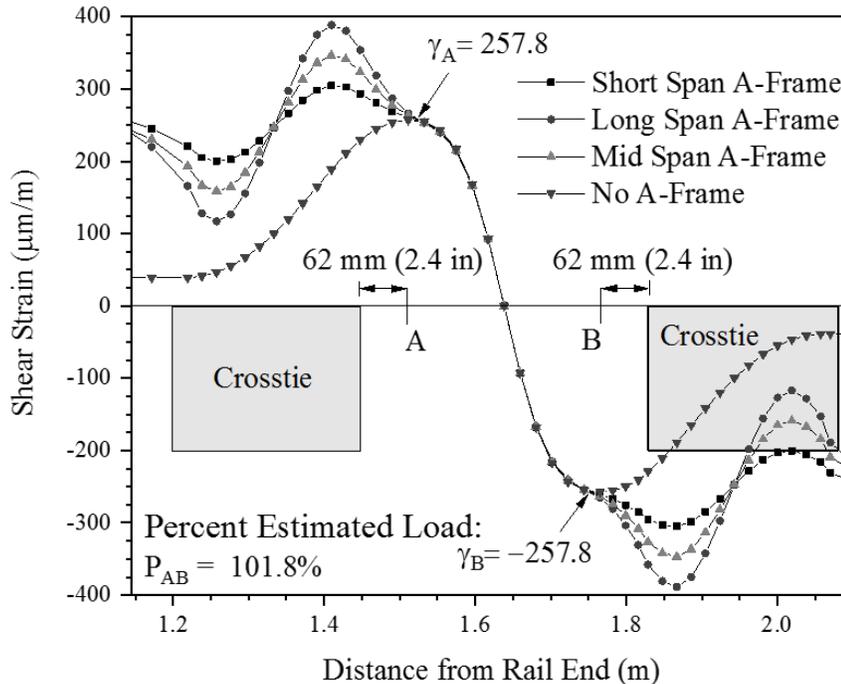

Figure 2.7 **Shear Strain Distribution at the Rail Neutral Axis Due to Loads Applied by Various A-Frame Configurations**

is independent of the A-frame used provided the strain gauges are properly located within the crib. At the ideal longitudinal locations for strain gauge placement, labelled A and B in Figure 2.7 (approximately 62 mm or 2.4 in. from the face of the adjacent crossties), the estimated load obtained for all A-frame configurations is 101.8% of the applied load. For gauges placed at a horizontal distance of less than 62 mm (2.4 in.) of the crosstie face, the type of A-frame used would have an impact on calibration. For example, at 38 mm (1.5 in.) from the crosstie face, the difference between the vertical load estimate using the long-span A-frame and the applied load is approximately 16%, whereas the difference between the load estimate using the short-span A-frame and the applied load would be 7.8%. This

shows the importance of properly placing the strain gauges within the crib prior to calibration.

Support Conditions

One of the implications of Figure 2.1 was that support conditions do not significantly impact the magnitude of the differential shear. As a final check of this conclusion and the Bernoulli-Euler beam assumption made in the associated shear analysis, the modulus of a portion of the ballast beneath a crosstie adjacent to the gauged crib section (Figure 2.4) was varied from 20 MPa to 230 MPa. As shown in Figure 2.8, the change in support condition leads to an asymmetrical distribution of shear strain with a reduction in shear strain near the weakly supported crosstie and an increase in shear strain near the normally supported crosstie. However, the percent estimated load for all three cases is
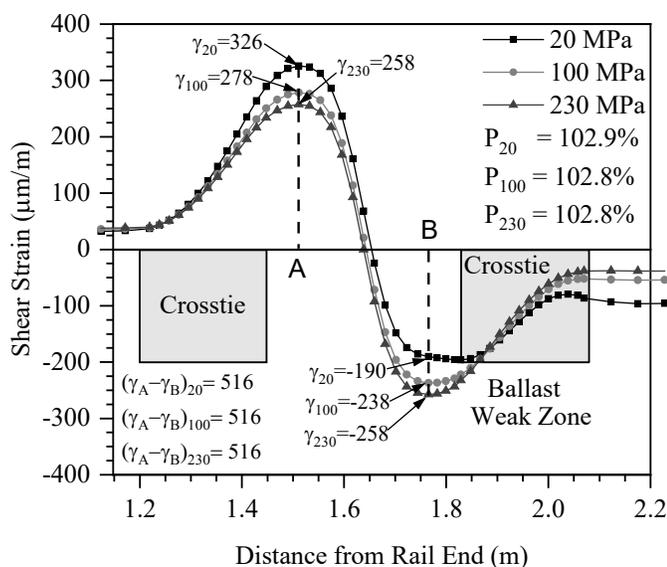

Figure 2.8   Impact of Support Conditions on Vertical Load Estimates

essentially unchanged (the difference in shear strains between points A and B is the same for all cases) validating that weakly or unsupported crossties do not significantly affect the accuracy of vertical load estimates.

Conclusions

This manuscript presented findings from an ongoing research study at Boise State University aimed at evaluating how different track configurations and loading conditions can affect the vertical load magnitudes backcalculated using the differential shear approach. A preliminary model of a 132RE rail section was developed and centrally loaded to compare the differences between the theoretical 2-D strain states with the 3-D behavior of physical strain gauge measurements under various loading conditions. It was found that loading conditions, primarily lateral loading conditions, do have an impact on the accuracy of strain gauge measurements. High lateral loads (L/V= 1) can reduce the accuracy of vertical load estimates by as much as 30%. However, these impacts are minimal for straight sections of track with low dynamic railcar/trackbed interaction. On curved track sections, adjustments to vertical load estimates could be made using additional circuits to measure lateral loads and using lateral loading data similar to the data in Table 2.1 to adjust measured vertical loads.

A layered elastic full-track FEM model was developed and analyzed to find the optimal strain gauge installation locations, and the impact of calibration techniques and support conditions on vertical load estimates. It was found that the optimal horizontal placement changes as crosstie spacing increases and the optimal vertical placement remains unchanged. Based on these results, the optimal horizontal placement from the crosstie face for a typical concrete tie spacing (610 mm center-to-center), is 62 mm (2.4 in.) from the crosstie face. Placing the gauges near this location leads to the optimal performance of the measurement circuit. Additionally, proper circuit placement within the crib ensures that strain gauge measurements are independent of geometric configuration of the calibration

equipment. Finally, it was validated that support conditions do not impact vertical load estimates. Current research efforts are focused on how differential shear measurements can be applied to quantify support conditions under crossties; relevant findings will be reported in future manuscripts.

CHAPTER THREE: MANUSCRIPT 2 — QUANTIFICATION OF VERTICAL AND
LATERAL LOADS USING STRAIN GAUGES – ELIMINATING THE
WHEATSTONE BRIDGE

Abstract

Real-time measurement of vertical wheel loads applied to the rail is commonly carried out using strain gauges. One standard approach involves measurement of shear strains at the rail neutral axis and use of the differential shear concept. Strain gauges are typically mounted on the rail neutral axis between two adjacent ties (over the crib section). A set of four strain measurements (two each, pointed at 45 degrees up and down from the horizontal) are carried out at each end of the crib section, and the measured strains are used to calculate the shear strain magnitudes; this shear strain is in turn used to calculate the applied load. In practice, the four individual strain measurements on each end of the crib (on either face of the rail) are arranged in a single Wheatstone bridge circuit. The purpose for using this common strain measurement configuration lies in the circuits' ability to eliminate crosstalk or strain unrelated to the load being measured, e.g., bending strain or strain due to lateral loading, etc. This paper will propose a new measurement approach whereby eliminating this Wheatstone bridge configuration and measuring eight independent strain signals will enable direct quantification of the vertical as well as lateral load magnitudes. Instead of having to install additional strain gauges on the rail base to measure the lateral loads, the same strain gauges mounted on the rail neutral axis can be

used to measure both vertical as well as lateral loads. This proposed technique will simplify

the process of vertical and horizontal wheel load detection and may increase the

applicability of these circuits to detect loads in curved sections of track as well as near

special track work.

Introduction

One of the most common wayside wheel load monitoring techniques employed in

the rail industry is to mount chevron-style strain gauges to the crib section of the rail. The

strains measured by these gauges are then related to applied wheel loads through rail

material and geometric properties. Due to crosstalk between vertical and lateral load-

induced strains, two separate strain circuits are employed: one for vertical load and one for

lateral load. The vertical load circuit comprises four chevron-style strain gauges placed at

the rail neutral axis (N/A) to measure strains at $\pm 45°$ as shown in Figure 3.1. Two gauges

are placed symmetrically about the crib center between the crib center and the face of

adjacent crossties on each face of the rail web. The distance D is chosen such that the

induced strains are not affected by the boundary effects of the load and crosstie supports

(Rabbi et al., 2019).
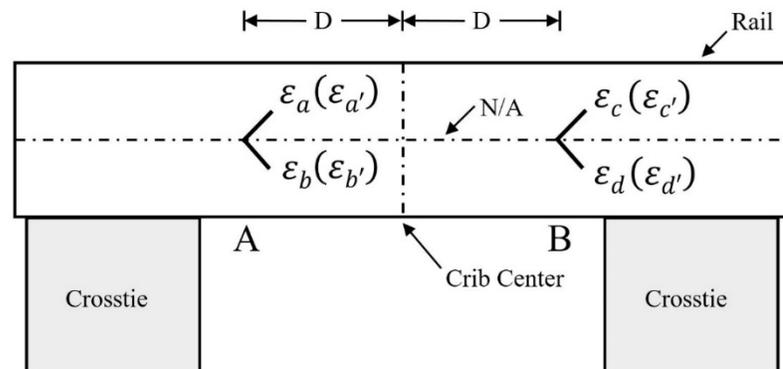
**Figure 3.1** **Typical Vertical Circuit Strain Gauge Configuration (ε_a, ε_b, ε_c and ε_d are shown; $\varepsilon_{a'}$, $\varepsilon_{b'}$, $\varepsilon_{c'}$ and $\varepsilon_{d'}$ are on the other face of the rail)**

The gauges are arranged in a single Wheatstone bridge configuration which eliminates the effects of lateral load (crosstalk) on the induced strains, and which outputs the difference in shear strain between locations A and B (see Figure 3.1). Differential shear is then directly proportional to the change in shear force caused by the applied load allowing for the determination of the applied load magnitude. A similar configuration is used for the lateral circuit. However, in the lateral circuit, the gauges are installed on the rail foot. The lateral load circuit uses the same principle of differential shear and a Wheatstone bridge circuit to eliminate the impact of the strains due to vertical loads. These methods were first presented by Ahlbeck et al. (1976) and are still in wide use today. Though Ahlbeck et al. (1976) presented a different variation of the lateral circuit described here, current lateral circuits are variants of the vertical load circuit presented in their report.

One of the primary functions of these circuits and the Wheatstone bridge configuration is to eliminate crosstalk so that the vertical and lateral loads can be measured independently. From the very initial days of wheel load measurement using strain gauges, the Wheatstone bridge has typically been incorporated into wheel load circuits and consequently the nature of crosstalk between vertical and lateral load-induced strains is relatively unknown. While engaged in a larger investigation into strain gauge-based wheel load measurements, different factors that impact these measurements, and the applicability of differential shear circuits in monitoring crosstie support conditions; it was observed that from a theoretical point of view, both lateral and vertical loads can be estimated from a linear combination of the eight (8) strains measured in the vertical load circuit. This study takes that theoretical observation and tests whether it is possible to measure both vertical and lateral load with a single vertical load circuit. If successful, the installation of wheel

load detection circuits could be improved by halving the number of strain gauges and circuits required. In addition, a better understanding of the nature of the crosstalk between vertical and lateral load-induced strains could provide insight into other relationships such as the interdependence of strain measurements on rail contact position.

Different methods have been identified that can successfully decouple wheel loads into their vertical and lateral components. One recent example of this was presented by Cortis et al. (2017). Building on the work of Moreau (1987), Cortis et al. (2017) proposed a new technique using rail bending strain to decouple vertical and lateral load components. It was found that this technique was able to accurately determine both vertical and lateral load with an error of less than 10% in a laboratory bench study. This approach certainly has merit and may represent the future of wheel load detection technology. However, it is hoped that a more open search, free of theoretical underpinnings (e.g. beam theory), may uncover other useful relationships which can increase the functionality of wheel load detection circuits. One potential example of this, as stated previously, could be the determination of contact position based on strain gauge measurements. Current efforts to investigate whether such relationships can be established are ongoing.

Research Objective and Scope

The primary objective of this research effort was to investigate the nature of vertical and lateral load crosstalk in differential shear circuits, and to find a quantitative relationship between the strains measured in the vertical load circuit and both vertical and lateral loads. As the Wheatstone bridge circuit is configured to eliminate such crosstalk, bridge behavior was not modeled in this effort. Instead, all eight (8) strain measurements are measured individually in a simple numerical parametric study. A simply supported section of

AREMA 132RE rail was modeled using the FEM software ABAQUS® as shown in Figure 3.2.
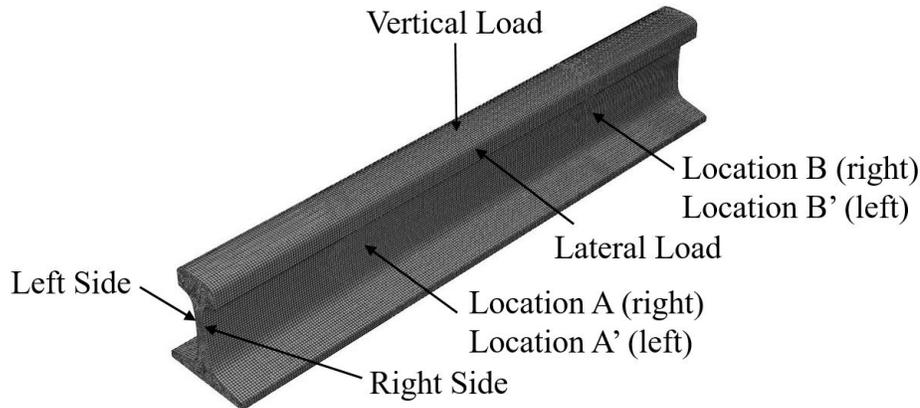

Figure 3.2   Simple FEM Model of AREMA 132RE Rail Section

The model used in the study was 1-m long and was centrally loaded with meshed combinations of vertical and lateral loads. A vertical point load was applied at the center of the rail crown, and a lateral point load was applied at the lower tangent of the crown fillet. The load combinations consisted of vertical and lateral loads ranging from 0 to 250 kN in increments of 10 kN resulting in a total of 625 simulations. Virtual strain gauges were placed at the neutral axis of the rail section at the longitudinal quarter points on both faces of the rail web. The virtual strain gauge comprised a 4 mm x 4 mm square element with a diagonal length (gauge length) of 5.7 mm. The type of element chosen for this model was the ABAQUS® 3D8I element which is a linear hexahedral element with additional internal degrees of freedom to reduce parasitic shear and artificial stiffening due to bending (ABAQUS, 2014). The nodal mesh was assigned a global size of 5 mm, and this configuration resulted in nearly cubical elements within the web of the rail. The properties used to define the model are summarized in Table 3.1.

Table 3.1   Simply Supported AREMA 132RE Model Properties

Parameter	Description
Length	1 m
Section	AREMA 132
Modulus of Elasticity	207 GPa
Poisson's Ratio	0.3
Element Type	C3D8I
Global Element Size	5 mm
Number of Elements	178,000
Restraint 1 (z = 0 m)	U1, U2
Restraint 2 (z = 1 m)	U1, U2, U3

Note: U1 = Lateral, U2 = Vertical, U3 = Longitudinal

Nodal displacements for each simulation were used to calculate the infinitesimal strain for virtual strain gauges defined by the diagonal surface nodes of the gauge element. Table 3.2 presents the strain output for three (3) select cases of vertical and lateral load. Based on prior observation, it was known that vertical and lateral loads could be accurately determined from a linear combination of the shear strain values output by the FEM model. However, as these values are theoretical in-plane values only, it was unclear as to whether this observation would hold for a physical strain gauge.

Table 3.2   Strain Output for Select Simulation Cases

Parameter	Case 1	Case 2	Case 3
Vertical Load (N)	-100000	-200000	0
Lateral Load (N)	0	-50000	-100000
ε_a	-1.27E-04	6.28E-05	7.14E-04
ε_b	1.30E-04	2.59E-04	3.53E-05
ε_c	1.30E-04	2.50E-04	1.49E-05
ε_d	-1.27E-04	3.52E-05	6.65E-04
$\varepsilon_{a'}$	-1.27E-04	-4.91E-04	-3.93E-04
$\varepsilon_{b'}$	1.30E-04	2.99E-04	1.14E-04
$\varepsilon_{c'}$	1.30E-04	3.06E-04	1.28E-04
$\varepsilon_{d'}$	-1.27E-04	-4.57E-04	-3.19E-04

As previously shown by Rabbi et al. (2017), the loads estimated from the in-plane component of shear strain can accurately establish the vertical load magnitude independent

of the lateral load magnitude. However, when using nodal displacements to estimate the 3D strain behavior of a physical gauge, increasing lateral load causes an increase in the error of vertical circuit load measurements. This behavior suggests an interdependence between vertical and lateral load that may or may not be linear. Therefore, a linear regression of the eight (8) strain measurements for each simulation was conducted to ascertain whether a linear relationship can be found to relate the strain measurements of the vertical load circuit to vertical and lateral load magnitudes.

Results

A linear regression analysis of the relationship between the applied vertical load and the strain measurements of the vertical load circuit shows that the relationship is indeed linear. Furthermore, the coefficient of multiple determination is unity meaning the vertical load can be precisely determined from the strain gauge outputs of the vertical load circuit.

This matches the aforementioned observation showing that a linear combination of strain gauge measurements can be found which provides the same behavior as the Wheatstone bridge: effectively eliminating crosstalk between vertical and lateral load. The following equation precisely calculates the vertical load independent of lateral load (with zero error, or $\epsilon=0$):

$$V = \beta_0 + \sum_{i=1}^{8} \beta_i x_i + \epsilon \qquad (3.1)$$

where,

V = Vertical load magnitude;

β_0 = Regression intercept;

β_i = Regression parameters;

x_i = Strain gauge measurements;

$x_i \in [\varepsilon_a \; \varepsilon_b \; \varepsilon_c \; \varepsilon_d \; \varepsilon_{a'} \; \varepsilon_{b'} \; \varepsilon_{c'} \; \varepsilon_{d'}]$ as defined in Figure 1

ϵ = Error.

A similar linear regression analysis for the relationship between lateral load and vertical circuit strain measurements shows a slightly more complicated relationship. The lateral load estimated from the strain measurements was found to be dependent on both lateral and vertical load magnitudes. For any given vertical load, a linear combination of vertical circuit strain gauge measurements can be found which will precisely calculate the lateral load. Therefore, the required relationship must also account for the 'interactions' between vertical load and strain measurements. This is done through a linear regression analysis which incorporates two-way interaction terms as shown below:

$$L = \beta_0 + \sum_{i=1}^{8} \beta_i x_i + \sum_{j=1}^{7} \sum_{k=2}^{8} \beta_{jk} x_j x_k + \epsilon, \text{for } j < k \qquad (3.2)$$

where,

L = Lateral load magnitude;

β_0 = Regression intercept;

$\beta_{i,jk}$ = Regression parameters;

$x_{i,j}$ = Strain gauge measurements;

$x_{i,j} \in [\varepsilon_a \; \varepsilon_b \; \varepsilon_c \; \varepsilon_d \; \varepsilon_{a'} \; \varepsilon_{b'} \; \varepsilon_{c'} \; \varepsilon_{d'}]$ as defined in Figure 1

ϵ = Error.

Here again, the coefficient of multiple determination is unity (ϵ=0) showing that the expression in Equation (3.2) is capable of precisely determining the lateral load

independent of vertical load magnitude. For the parametric study described above and shown in Figure 3.2, the regression parameters in Equations (3.1) and (3.2) are shown in Table 3.3.

Table 3.3   Linear Regression Parameters with Two-Way Interactions

Gauge	β Vertical Load (N)	β Lateral Load (N)	Gauge	β Lateral Load (N)
$x_0 = 1$	-12	-4.0715E-02	$x_b x_{a'}$	-8.5704E+10
x_a	1.3885E+09	-6.2480E+07	$x_b x_{b'}$	0
x_b	-3.4463E+08	2.2896E+07	$x_b x_{c'}$	4.3547E+10
x_c	7.7650E+08	-5.1063E+07	$x_b x_{d'}$	0
x_d	-1.1254E+09	-7.2743E+07	$x_c x_d$	-3.7191E+10
$x_{a'}$	1.3675E+09	2.6572E+07	$x_c x_{a'}$	0
$x_{b'}$	-1.2190E+08	-2.6654E+07	$x_c x_{b'}$	0
$x_{c'}$	-7.1132E+08	-2.2758E+07	$x_c x_{c'}$	0
$x_{d'}$	-1.2544E+09	2.9704E+07	$x_c x_{d'}$	0
$x_a x_b$	0	3.4148E+09	$x_d x_{a'}$	1.4995E+10
$x_a x_c$	0	-1.6358E+10	$x_d x_{b'}$	6.1634E+08
$x_a x_d$	0	1.5809E+10	$x_d x_{c'}$	-1.2832E+10
$x_a x_{a'}$	0	-1.7590E+10	$x_d x_{d'}$	-2.3181E+10
$x_a x_{b'}$	0	-2.6890E+09	$x_{a'} x_{b'}$	4.8947E+10
$x_a x_{c'}$	0	0	$x_{a'} x_{c'}$	1.6995E+10
$x_a x_{d'}$	0	-2.7624E+09	$x_{a'} x_{d'}$	4.1558E+10
$x_b x_c$	0	4.4926E+10	$x_{b'} x_{c'}$	0
$x_b x_d$	0	0	$x_{b'} x_{d'}$	-3.3830E+10
			$x_{c'} x_{d'}$	0

Note: $x_a = \varepsilon_a$, and term $x_a x_{d'}$ is the multiplication of ε_a and $\varepsilon_{d'}$ as defined in Figure 3.1

Referring to the strain values presented in Table 3.2, for Case # 2 (V = -200 kN, L = -50 kN), and the regression parameter presented Table 3.3, an example of the vertical and lateral load determination is presented in Table 3.4 on the following page.

Table 3.4   **Example Vertical & Lateral Load Calculations**
(V=-200 kN, L=-50 kN)

x-term	x-term value	β (Vertical)	β (Lateral)	Total Term (Vertical; N)	Total Term (Lateral; N)
$x_0 = 1$	1	-12	-4.0715E-02	-12	-4.07E-02
x_a	6.27930E-05	1.3885E+09	-6.2480E+07	8.7188E+04	-3.92E+03
x_b	2.58919E-04	-3.4463E+08	2.2896E+07	-8.9231E+04	5.93E+03
x_c	2.49515E-04	7.7650E+08	-5.1063E+07	1.9375E+05	-1.27E+04
x_d	3.52235E-05	-1.1254E+09	-7.2743E+07	-3.9641E+04	-2.56E+03
$x_{a'}$	-4.90585E-04	1.3675E+09	2.6572E+07	-6.7087E+05	-1.30E+04
$x_{b'}$	2.98653E-04	-1.2190E+08	-2.6654E+07	-3.6406E+04	-7.96E+03
$x_{c'}$	3.06360E-04	-7.1132E+08	-2.2758E+07	-2.1792E+05	-6.97E+03
$x_{d'}$	-4.56920E-04	-1.2544E+09	2.9704E+07	5.7316E+05	-1.36E+04
$x_a x_b$	1.625830E-08	-	3.4148E+09	-	5.55E+01
$x_a x_c$	1.566780E-08	-	-1.6358E+10	-	-2.56E+02
$x_a x_d$	2.211789E-09	-	1.5809E+10	-	3.50E+01
$x_a x_{a'}$	-3.080530E-08	-	-1.7590E+10	-	5.42E+02
$x_a x_{b'}$	1.875332E-08	-	-2.6890E+09	-	-5.04E+01
$x_a x_{d'}$	-2.869138E-08	-	-2.7624E+09	-	7.93E+01
$x_b x_c$	6.460417E-08	-	4.4926E+10	-	2.90E+03
$x_b x_{b'}$	7.732694E-08	-	-8.5704E+10	-	-6.63E+03
$x_b x_{d'}$	-1.183053E-07	-	4.3547E+10	-	-5.15E+03
$x_c x_{a'}$	-1.224083E-07	-	-3.7191E+10	-	4.55E+03
$x_d x_{b'}$	1.051960E-08	-	1.4995E+10	-	1.58E+02
$x_d x_{c'}$	1.079107E-08	-	6.1634E+08	-	6.65E+00
$x_d x_{d'}$	-1.609432E-08	-	-1.2832E+10	-	2.07E+02
$x_{a'} x_{b'}$	-1.465147E-07	-	-2.3181E+10	-	3.40E+03
$x_{a'} x_{c'}$	-1.502956E-07	-	4.8947E+10	-	-7.36E+03
$x_{a'} x_{d'}$	2.241581E-07	-	1.6995E+10	-	3.81E+03
$x_{b'} x_{c'}$	9.149533E-08	-	4.1558E+10	-	3.80E+03
$x_{c'} x_{d'}$	-1.399820E-07	-	-3.3830E+10	-	4.74E+03
			Sum:	-199987.64	-50000.01
			% Error:	0.0062%	-0.000026%

The relationships between vertical circuit strain gauge measurements and the magnitude of vertical and lateral load presented here are for a single load position. It is likely that as the load contact point moves, the values of the regression parameters shown in Table 3 will change. Additional work is required to investigate how the regression parameter values change as a function of load position. To implement this theoretical

relationship in the field, it may be necessary to find a relationship between longitudinal load position and strain gauge measurements. One way to avoid this is to employ signal processing techniques capable of identifying the time at which the load is at a specific point within the gauged section, e.g., at the crib center. Using this approach, the regression constants presented in Table 1 should provide 'fair' estimates of wheel loads as there is some error (though small) associated with the lateral contact position. A quantification and correction of this error is another current area of investigation. In addition, the impact that support conditions (e.g., crossties and fastening systems) have on vertical strain circuit measurements will also need to be investigated. Finally, the method proposed here may not represent a significant improvement to current load sensing technology. This will largely depend on the signal conditioning and post processing costs associated with processing eight (8) signals as opposed to only two (2); simply halving the number of gauges required does not guarantee a reduction in total cost. However, the ability to determine lateral load, vertical load and potentially the load position could provide a significant functional improvement that may justify any additional infrastructure costs.

Summary and Conclusion

This manuscript presented findings from an ongoing research effort aimed at discovering relationships between the strains measured in a vertical wheel load detection circuit and the applied vertical and lateral loads. To investigate the nature of the interdependence (crosstalk) between vertical loads, lateral loads and strain gauge measurements, the Wheatstone bridge circuit was removed, and individual strain gauge measurements were analyzed. A parametric study of 625 load combinations of vertical and lateral load, ranging between 0 and 250 kN, was conducted on a simply supported section

of AREMA 132RE rail. The induced strains from each simulation were used in a linear regression analysis to find a quantitative relationship between wheel-load induced strains and the corresponding magnitudes of vertical and lateral loads. It was found that a linear combination, including two-way interaction terms, of the eight (8) strain gauge signals in a typical vertical wheel load circuit was able to accurately determine both the vertical and lateral load magnitudes when the load position remains laterally and longitudinally constant. Additional work, in the form of laboratory or field verification tests, is required to assess whether the method presented here is viable for field implementation or not. Current research efforts are aimed at finding an additional relationship to account for the longitudinal position of the applied load. If successful, typical vertical circuit gauge configurations can be used (sans the Wheatstone bridge) to simultaneously determine the vertical load, lateral load, and wheel load contact position, providing a time-history of wheel load as it passes through the circuit.

CHAPTER FOUR: USING DIFFERENTIAL SHEAR STRAIN MEASUREMENTS TO

MONITOR CROSSTIE SUPPORT CONDITIONS IN RAILROAD TRACKS

Introduction

With the validity of the differential shear strain method verified on a theoretical

basis in the first paper, and with an increased understanding of the response of rail shear

strain to vertical and lateral load, gained through the efforts of the second paper, the final

task was to answer the remaining research question: whether the approach used by

Tutumluer et al. (2015) is valid from a theoretical standpoint. One approach to answering

this question is to leverage the relationship in Equation 3.1 between shear strain measured

in the vertical load circuit and the applied load. If the relationship between circuit strain

response and applied load remains unchanged regardless of whether the circuit is a crib

circuit or a crosstie circuit, then the primary differences between the two circuits, i.e.

different loading conditions and deflected shape due to rail pad/crosstie reaction, do not

significantly impact the output of the circuit. Therefore, it would be theoretically valid to

apply the calibration curve determined in an adjacent crib circuit to the crosstie circuit, as

was done in Tutumluer et al. (2015). This is important for the practicality of the method as

calibrating the crosstie circuit would require inserting a load cell between the rail and

crosstie; considered impractical for routine use by field practitioners.

Research Approach

To determine whether the calibration curve from the crib circuit can be used to

calibrate the crosstie circuit, the full-track FE model developed in Chapter 2 was modified

and loaded at the crib circuit under various vertical load magnitudes to determine the regression coefficients in Equation 3.1. With these coefficients determined, the crosstie circuit was subsequently loaded, and Equation 3.1 was used to estimate the applied load. Close agreement between the crosstie reaction at the crosstie circuit and the estimated crosstie reaction using the coefficients determined from the crib circuit would prove that the differences between the two circuits are not significant in the determination of applied load. This implies that the calibration curve, or the relationship between applied load and strain response, from the crib circuit can be used to calibrate both circuits.

Modifications to the full track FE model developed in Chapter 2 were made to better represent field conditions typical of highspeed rail applications as shown in Figure 4.1. The model was expanded to include nine crossties. This change was made as unwanted
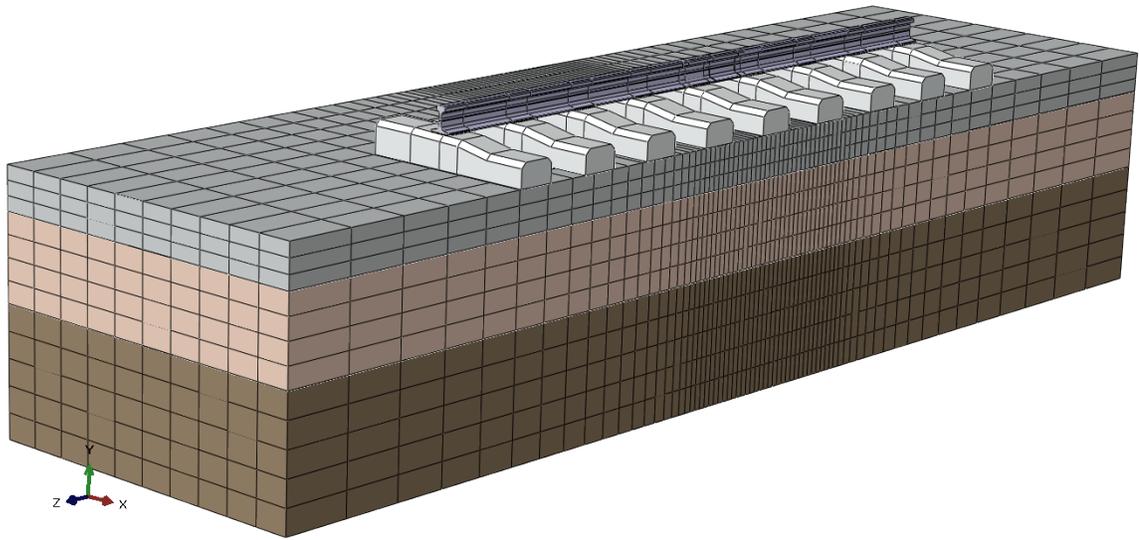

Figure 4.1   Expanded Full-Track FEM Model

boundary conditions (deflections at the outermost crossties) from the previous model comprised of seven crossties had been observed, and it was hoped that expanding the model would help to improve these conditions. The crossties were also modified to represent the

geometry of typical crossties used in highspeed rail applications as shown in Figure 4.2, and to add rail cant to the model to investigate the impact of rail cant on load determination.
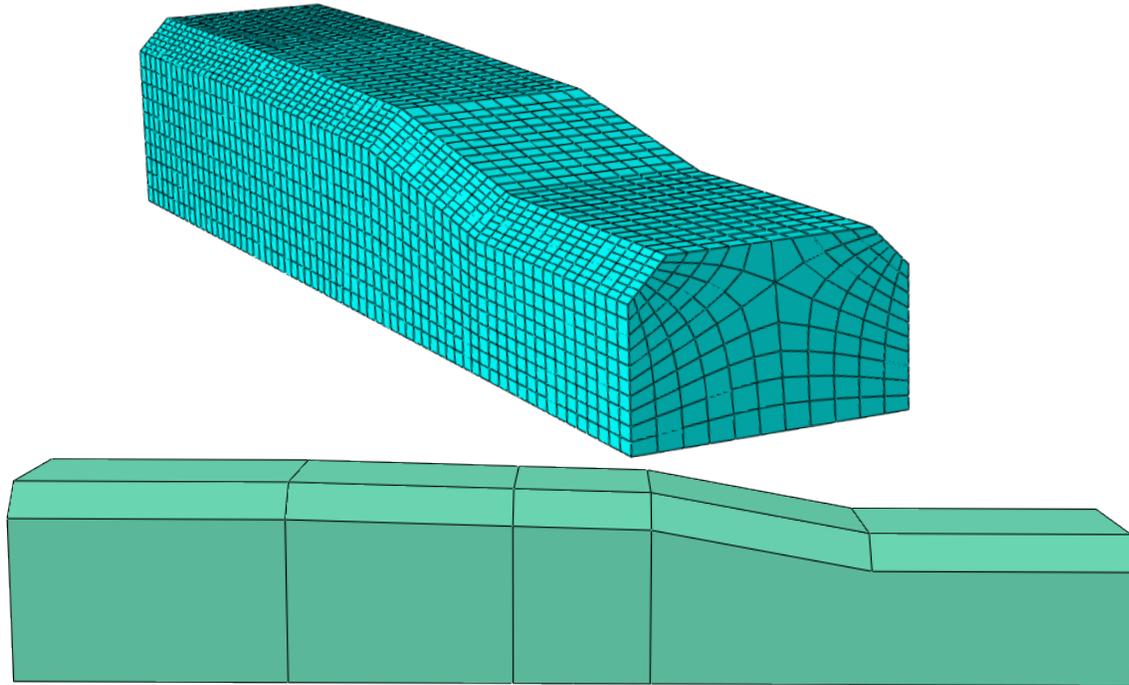

Figure 4.2   Concrete Crosstie Geometry and Meshing

The 5 mm thick rail pads shown in Figure 4.3 were defined with an elastic modulus of 5 MPa and a Poisson's ratio of 0.45. These pads were added to the model with a frictional contact interaction between the rail and rail pad. The frictional contact was defined as a surface-to-surface contact using a penalty formulation and a frictional coefficient of 0.64 which is a typical value for rubber/steel contact. The purpose of this modification was to model the interaction between the rail and rail pad. As the rail deflects under load, the rail will tend to bend away from the surface of the rail pad. In the previous models, a tie constraint was defined for the rail/crosstie interface. However, this type of constraint may have an impact
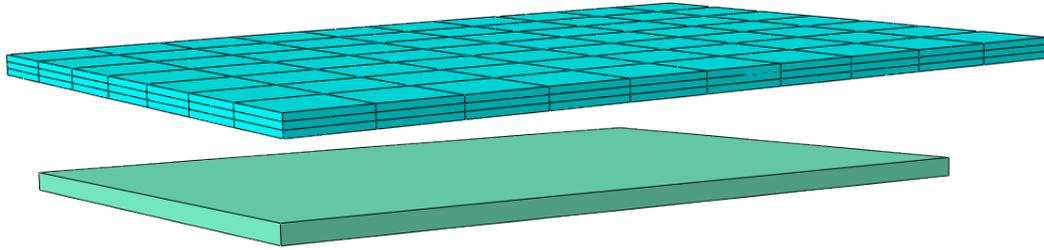
Figure 4.3   Rail Pad Geometry and Meshing

on the rail deflected shape (and corresponding shear strain) as it constrains the rail from

lifting away from the crosstie as the rail deflects under load. The point of loading was also

moved inward from the rail section center to the top of the inside rail section fillet as shown

in Figure 4.4 for both crib and crosstie circuit loading. This location is similar to the actual

wheel/rail contact area and provides a better representation of actual wheel loading
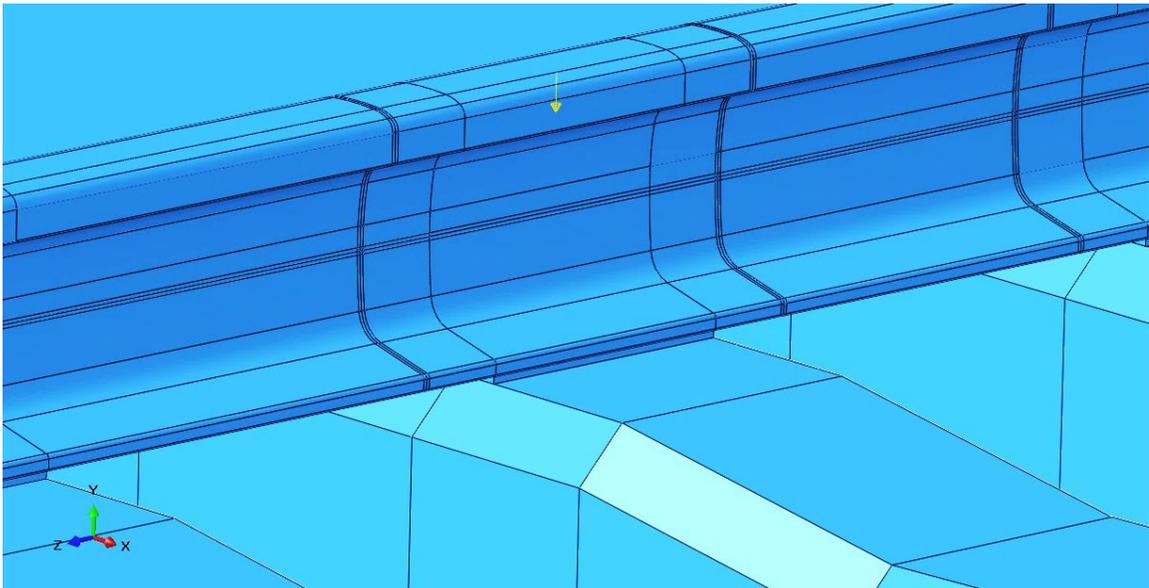
Figure 4.4   Point of Load Application

conditions. It should be noted that circular and oval contact pressures were also applied to

the rail in some model simulations resulting in no appreciable differences in shear strain

response from simulations with concentrated point loading. These simulations have

accordingly been omitted for brevity. With all the model changes discussed above, the modified model was comprised of 545,370 model elements.

Finally, with the analysis of the crosstie circuit load/strain response complete, the sensitivity of the crosstie circuit to changing crosstie support conditions was investigated. Similar to the approach used in Chapter 2, a 'weak zone' of variable strength was created under the crosstie. The track was then loaded as the strength of the weak zone was varied and the percent support was estimated using the approach adopted by Mishra et al. (2015) as follows:

$$R = P - (P - R) = \frac{EIt}{2Q(1 + v)}(\Delta\gamma_c - \Delta\gamma_x) \tag{4.1}$$

where

R = crosstie reaction;

$\Delta\gamma_c$ = differential shear strain measured in the crib shear circuit (see Figure 1.1);

$\Delta\gamma_x$ = differential shear strain measured in the crosstie shear circuit (see Figure 1.1)

The percent support, S, or percentage of the applied load supported by the crosstie is then:

$$S = \frac{R}{P} \times 100\% = \frac{\Delta\gamma_c - \Delta\gamma_x}{\Delta\gamma_c} \times 100\% \tag{4.2}$$

For an ideal completely rigid crosstie support, the crosstie reaction is equal to the applied load and percent support is 100%. Conversely for a completely unsupported crosstie, the crosstie reaction disappears, and the percent support is 0%.

Results

As shown in Figure 4.5, with a scale factor of 200, the revise contact interaction described
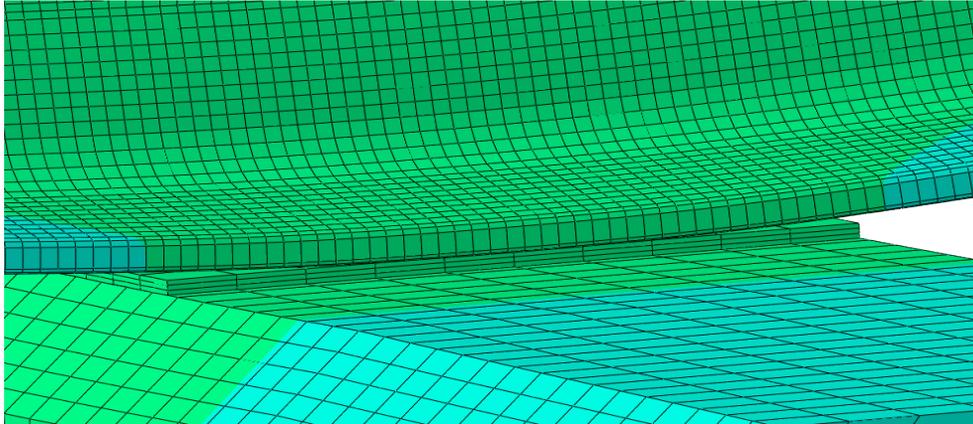

Figure 4.5   Rail Deflection Under 100 kN Load at the Inside Foot of the Rail

previously allows the rail to deflect away from the rail pad resulting in a more representative deflected shape. However, this is still an over-simplification of actual field conditions as the interaction of the rail clip and its corresponding impact on the deflected shape of the rail is not modeled. The difference between the deflected shape of the rail between the crib and crosstie circuits is shown in Figure 4.6, again at a scale factor of 200. The area of exaggerated vertical deflection shown in these figures is due to the singularity
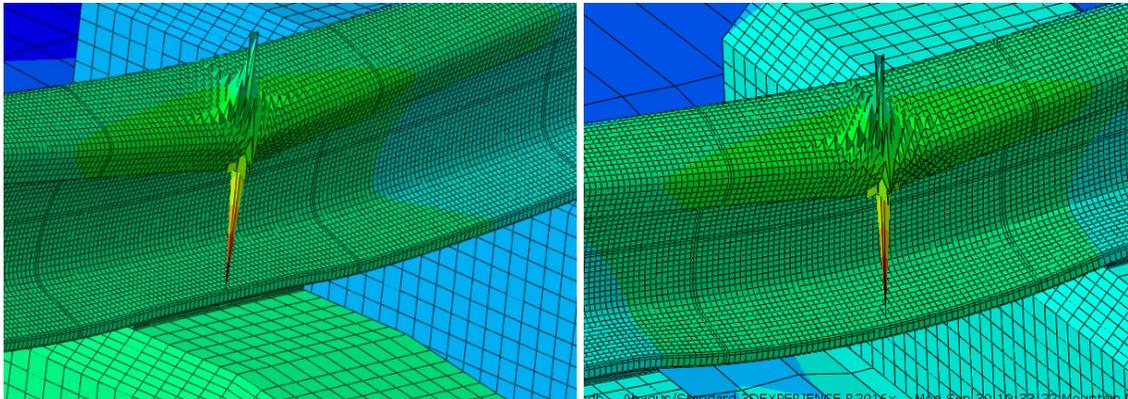

Figure 4.6   Rail Deflection Under 100 kN Load for Crosstie (Left) and Crib (Right) Circuits.

introduced from the concentrated point load. Due to this singularity, local strain magnitudes are unreliable. However, this boundary condition does not significantly impact the accuracy of strain values in the area of interest for this study. As the figure shows, there are significant differences in the deflected shape of the rail under load between these two circuits. It is these differences in deflected shape that may cause errors when using the Crib circuit calibration to calibrate the crosstie circuit.

As discussed previously, to determine whether or not these differences in deflected shape lead to significant differences in strain response between the two circuits, a parametric analysis of the crib circuit was conducted to determine the regression coefficients of Equations 3.1. Table 4.1 lists the load magnitudes used in the parametric analysis along with the associated regression coefficients. The crosstie circuit was then

Table 4.1   **Crib Circuit Parametric Regression Analysis**

Crib Parametric Loading (kN)	Crib Regression Parameters	
50	β_0	-3.45E-11
100	β_a	-1.15E+08
150	β_b	0
200	β_c	1.33E+08
250	β_d	-2.74E+07
300	$\beta_{a'}$	-1.93E+08
350	$\beta_{b'}$	-1.50E+07
	$\beta_{c'}$	2.74E+08
	$\beta_{d'}$	0

loaded with a 100 kN load in four (4) scenarios of varying ballast strength. Crosstie reactions were calculated using the regression parameters in Table 4.1 and these values were compared with direct crosstie reaction measurements. As shown in Figure 4.7, the percent support predicted by Equation 3.1 is within approximately 2% of measured values.

underlying ballast, reducing the impact of ballast stiffness. However, as the strength of the support continues to drop, the percent support begins to drop significantly. This result shows that the sensitivity of the circuit may be more suited to assessing large changes in support strength, especially for detecting hanging or unsupported crossties. Extensive field validation would be required to determine if changes in percent support using this method are sensitive enough to make useful predictions of ballast strength.

Another implication of 4.7 is that, if the differences in deflected shape between the crib and crosstie circuits don't have a significant impact on shear strain values, it may be possible to use the crosstie circuit alone to predict subgrade strength without the use of a separate crib circuit. A regression analysis trained on load and overall ballast/subgrade strength may be able to provide suitable relationships to predict not only load, but also subgrade support strength without separately determining vertical load in the crib circuit. To test this hypothesis, the model in Figure 4.1 was loaded with a 100kN vertical load under the same ballast strength parameters used in Figure 4.7 (50, 100, 150, and 230 kN, respectively). The corresponding crosstie circuit shear strain values were used in another regression analysis to find a relationship between stain values under a known load to crosstie support strength. The results of this analysis established that fairly accurate predictions of ballast strength can be made using quadratic Support Vector Machines (SVM) trained on shear strain response under known load. As shown in Figure 4.8, this approach provided an RMSE value of 19.77 MPa and a Coefficient of Determination value of 0.95. Thus, ballast strength predictions using machine learning can theoretically be used for assessing track support conditions. A series of SVM models can be trained on a large

range of expected vertical load values and these models can then be used in postprocessing

algorithms to determine crosstie support strength based on measured vertical load. To
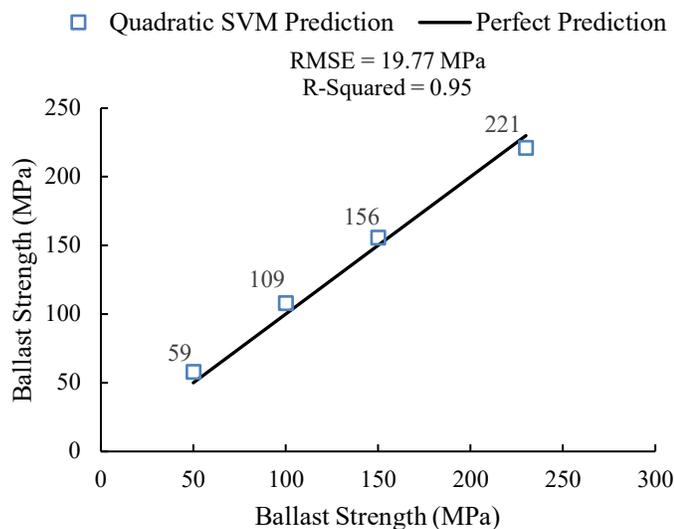
**Figure 4.8   SVM Predictions of Ballast Support from Strain Gauge
Measurements under 100kN Vertical Loading**

measure the vertical load, Equation 3.1 can be used with the coefficients determined from

the shear strain response of the crosstie circuit rather than the crib circuit. A much more

powerful potential approach would be to use a multivariate regression analysis using both

load and ballast strength responses. If a reasonably accurate multivariate regression model

could be found however, the approach would still require a lengthy parametric analysis to

obtain a large database of strain values (predictor variables) under various load and ballast

strength combinations (response variables) which is beyond the scope of this research

effort. It should be noted that this approach would also require further analysis over various

other track parameters such rail section geometry, tie spacing, rail/tie connection

configurations, etc. to make these predictions globally valid over a large range of railroad

track configurations. However, the approach does demonstrate the power of post-

processing all eight strain gauge outputs (as opposed to combining them in a Wheatstone bridge) to determine vertical, load, lateral load, and crosstie support conditions.

Conclusion

This numerical investigation primarily dealt with determining whether the approach used by Tutumluer et al. (2015) to assess and monitor crosstie support conditions was valid. The approach used an additional crosstie circuit to monitor percent crosstie support, and to calibrate this additional circuit with the calibration curve determined from the adjacent crib circuit. It was found that this approach is valid from a theoretical standpoint. However, laboratory or field instrumentation is required to validate this conclusion under changing field conditions. Additionally, the sensitivity of the method was found to be limited for relatively stiffly supported crossties. However, as crosstie support continues to diminish, the approach provides an effective method for assessing weakly supported crossties. Additionally, it was found that quadratic SVM predictions of ballast strength based on the eight (8) strain gauge responses under known load are reasonably useful in assessing crosstie support conditions.

CHAPTER 5: SUMMARY, CONCLUSION AND RECOMMENDATIONS FOR

FUTURE RESEARCH

This thesis details an investigation of the use of strain gauges to determine wheel loads and crosstie support reactions in railroads using finite element methods. The use of strain gauges to measure applied loads first began in the 1970's and is still widely used today in WILD systems and other load sensing devices, and in various research efforts to determine rail/railbed interactions. Strain gauges are placed near the neutral axis of the rail web to measure vertical load, and on the rail foot to measure lateral load. As a wheel passes through the instrumented section of track, differential shear is measured and related to applied loads. Tutumluer et al. (2015) modified the method to include an additional circuit encompassing an adjacent crosstie. By measuring the difference in loads between these two strain gauge circuits, crosstie reactions were estimated and used to assess track stiffness and the level of crosstie support provided by underlying ballast and subgrade materials. However, questions regarding the accuracy of the method were raised in the industry. The impact of various field conditions on crosstie reaction measurements were unknown and the methods used to calibrate the crosstie circuit had yet to be validated. The specific purpose of the numerical investigations detailed in this thesis was to answer these primary questions.

Summary

Manuscript 1: Effect of Track Configuration and Loading Conditions on Vertical Wheel

Load Measurements Using the Differential Shear Approach

Several finite element models were developed and analyzed to test the theoretical validity of various aspects of the differential shear strain approach, beginning from a basic 1-D analysis of a beam on spring supports; and progressing to models of simply supported rail geometries and to full-track models representative of typical parameters measured in the field. The models were loaded under a range of material and geometric configurations and under various load combinations. The induced shear strains were then used to estimate applied vertical load and to assess the impact that these various factors have on the accuracy of vertical load estimates.

The investigation began with several analyses aimed at gaining a solid theoretical understanding of the underlying mechanics involved in the differential shear method. First, a 1-D beam on both rigid and spring supports was loaded to see how support compliance impacts shear force distribution along the beam (Figure 2.1). Additionally, one support was removed from the model leading to asymmetrical load/support conditions to investigate the impact of loosely supported or 'hanging' crossties.

Next, the theoretical shear strain state of a rail section under load was presented (Figure 2.2) and used to discuss the theory behind using differential shear strain measurements to determine applied loading. With the theoretical underpinnings behind the approach laid out, the impact that various loading combinations have on the accuracy of load determination was investigated. A simply supported AREMA 132RE rail section was loaded under various vertical, lateral, and axial loading combinations and induced shear

strains were then used to estimate the applied vertical loads to compare how these combinations impact the accuracy of vertical load estimates (Table 2.1).

To gain a better understanding of the proper installation configuration of strain gauges for the measurement of vertical load, the distribution of induced shear strain of three simply supported rail sections: AREMA 115RE, 132RE and 141RE under vertical load was used to estimate applied load. The percentage of estimated load vs. applied load was then plotted on the web of the rail sections (Figure 2.5) to locate areas of high load prediction accuracy.

The impact that crosstie spacing may have on vertical load estimates was investigated using a full-track model consisting of seven (7) crossties and typical ballast and subgrade strength values. Models using crosstie spacings of 19, 24, and 31 inches respectively were developed and the shear strain distribution along the longitudinal axes of the rail was plotted (Figure 2.6). Additionally, calibration load frames with different geometric configurations were modeled and used to load the rail. The induced shear strains under these various load-frame configurations were plotted (Figure 2.7) to investigate the impact that these load frame configurations have on vertical circuit calibration and associated vertical load estimates. Finally, the impact of weakly supported crossties was investigated by creating a 'weak zone' or an area of reduced ballast strength in the full-track model. The model was then loaded, and the strain distribution was plotted (Figure 2.8) and used to calculate estimated load.

Manuscript 2: Quantification of Vertical and Lateral Loads Using Strain Gauges—

Eliminating the Wheatstone Bridge

The next task in the investigation was to explore the interaction of vertical and lateral load in the strain gauge circuit. As typical instrumentation procedure is to combine all four gauges at each end of the circuit into a full Wheatstone bridge circuit and thereby eliminate crosstalk between vertical and lateral load, it was necessary to conduct this investigation without modeling the behavior of the full bridge. Instead, nodal deformations were used to model eight individual strain gauges (four at each end). A parametric study of a simply supported rail section under various combinations of vertical and lateral load was performed (Table 3.2) and the resulting shear strain data was used in a linear regression analysis to find relationships between induced shear strain and both vertical and lateral load, Equations 3.1 and 3.2 respectively. The regression coefficients in these equations were determined and presented in Table 3.3 and used in a test case to determine the accuracy of these relationships using measured shear strain values (Table 3.4).

Using Differential Shear Strain Measurements to Monitor Crosstie Support Conditions in

Railroad Tracks

The final task in the analysis was to validate the approach used by Tutumluer et al. (2015) to assess and monitor crosstie support conditions. First, another parametric study was performed on a full-track model revised to more closely represent typical field conditions found in highspeed rail applications. The model was then loaded under several loading scenarios to measure the load/strain response of the crib circuit. Using the measured strains, a linear analysis was conducted to determine the coefficients of Equation 3.1 (Table 4.1). Next, the crosstie circuit was loaded, and crosstie reactions were

determined from Equation 3.1 and compared to the measured crosstie reactions output from the FE model (Figure 4.7). Finally, the shear strain values under known load (from the previous analysis) were used to as predictor variables along with ballast strength values used as response variables in a linear regression analysis to find a predictive relationship between measured strain values under a known load and ballast strength.

Conclusion

<u>Manuscript 1: Effect of Track Configuration and Loading Conditions on Vertical Wheel Load Measurements Using the Differential Shear Approach</u>

From the analysis of a simple 1-D beam on rigid and spring supports (Figure 2.1), shear forces imparted to a rail section from an applied load remain constant between any two supports and the difference in internal shear force on either side of an applied load are equal to the applied load through a simple force balance. By using strain gauges and measuring induced shear strains on either side of the applied load, the load magnitude can be determined through rail geometric and constitutive properties.

By loading a simply supported 132RE rail section under various combinations of vertical, lateral, and axial load, it was found that axial load has very little impact on the accuracy of vertical load determination. However, due to interactions between vertical and lateral load in vertical load circuits, lateral load was found to have a significant impact on applied load estimates (Table 2.1).

An analysis of the accuracy of load determination based on strain gauge installation location (Figure 2.5) shows the impact of boundary conditions on the accuracy of load determination. The largest boundary impact is at the point of loading with much smaller impacts near the crosstie supports. The ideal placement location of strain gauges was found

to be approximately 2.5 inches from the face of the crosstie support near the neutral axis for vertical load determination.

Crosstie spacing was found to have little impact on the accuracy of vertical load measurements (Figure 2.6). However, spacing less than 19 inches will lead to errors due to the boundary effects of closely spaced crossties. Calibration load frame geometries do not have a significant impact on induced shear strain values (Figure 2.7) and associated calibration curves indicating that accurate vertical load measurements can be made regardless of the load-frame used to calibrate the circuit. It was also found that differential ballast support between crossties does not impact vertical load measurements (Figure 2.8). In summary, it was found that none of the factors above have a significant impact on the accurate measurement of vertical load using strain gauges. These results are consistent with field data as the determination of vertical load using strain gauges has long been found to be a robust measurement method.

Manuscript 2: Quantification of Vertical and Lateral Loads Using Strain Gauges—
Eliminating the Wheatstone Bridge

As shown in Table 3.4, the coefficients of equation 3.2 determined in a linear regression analysis of induced shear strain values from a simply supported 132RE rail section exactly predict both vertical and lateral load. For vertical load, the interaction terms in the linear regression are all zero indicating vertical load determination is unaffected by lateral load. However, for lateral load determination, these interaction terms are necessary to predict the load. This result is consistent with previous results in this thesis where it was found that lateral load determination is impacted by vertical load. It should be noted that the coefficients in the linear relationships presented herein do not provide a global

relationship for all railroad tracks but are instead local results potentially impacted by track stiffness and other field conditions.

Using Differential Shear Strain Measurements to Monitor Crosstie Support Conditions in Railroad Tracks

As shown in Figure 4.7, load estimates made using the load/strain response of the crib circuit (Table 4.1) can accurately predict the applied load when applied to the crosstie circuit. Thus, the calibration curve from the adjacent crib circuit can be used to calibrate the crosstie circuit without negatively impacting the accuracy of vertical load measurements. This result validates the method used by Tutumluer et al. (2015) to measure crosstie reactions. However, Figure 4.7 also indicates that large changes in ballast strength have only limited impact on crosstie reaction magnitudes for relatively well supported crossties. This indicates the method, while able to accurately predict crosstie support reactions, has limited ability to assess changes in ballast support strength over time and may only be suitable in assessing weakly supported or hanging crossties.

However, crosstie reactions can be accurately predicted by using the load/strain response of the crib circuit and therefore, the differences in loading conditions and deflected shape between the crib and crosstie circuits do not significantly impact the induced strains. Thus, it is possible to directly determine applied load from the crosstie circuit alone by calibrating the crosstie circuit using the same methods used to calibrate the crib circuit. In addition, once applied load is determined from the strain response of the crosstie circuit, it is also possible to make reasonable predictions of ballast strength under known load using a machine learning approach as shown in Figure 4.8. This final result highlights the power of postprocessing all eight (8) strain gauge outputs separately using

machine learning algorithms. It is reasonable to conclude (though not specifically verified herein) that this approach would be capable of determining vertical load magnitude, lateral load magnitude, and ballast support strength from the crosstie circuit output.

Recommendations for Future Research

Two major implications of this research effort are related to the crib and crosstie circuits respectively. For the crib circuit, based on Equations 3.1 and 3.2, it is possible to determine both vertical and lateral load with a single circuit rearranged to separately output all eight (8) strain gauge outputs. However, the practicality of doing this in the field needs to be investigated, and it is unclear if this approach would provide any significant advantage over the current practice of using separate circuits to process vertical and lateral load. Also, the coefficients of Equation 3.1 and 3.2 would need to be determined for each circuit installation as the coefficients presented in this thesis are local to the model used (a simply supported rail section). A large parametric study of various material, geometric and loading conditions corresponding to expected field conditions may be able to provide a set (or sets) of globally valid coefficients making field calibration unnecessary.

The same approach to determining vertical and lateral load may also be used in the crosstie circuit. By determining the coefficients of Equation 3.1 and 3.2 from loading the crosstie circuit under known vertical and lateral load magnitudes, it would be possible to determine both load magnitudes from eight (8) separate strain gauge measurements. Again, with a large parametric study over various expected track conditions, these coefficients could potentially be made global rather than local to each installation. In addition, once vertical load has been determined, it is possible to apply a linear regression model to the strain measurements to make reasonable assessments of ballast strength similar to the

approach used in Figure 4.8. However, a much larger parametric study would be required to find linear regression models of ballast strength under known load for a large range of expected load magnitudes. A much more powerful approach would be to use a multivariate machine learning approach to determine a single regression model to predict both vertical load and ballast strength. However, the existence of such a relationship in unknown.

Finally, exhaustive field instrumentation and measurement is recommended to validate the theoretical findings of this thesis and provide globally valid relationships over a variety of railroad track field conditions such as rail section material and geometric properties, crosstie spacing, crosstie geometric and material properties, rail pad and rail clip configurations, and ballast/subgrade support strengths.

REFERENCES

ABAQUS. 2014. *Abaqus V. "6.14 Documentation".* Dassault Systèmes, Simulia Corporation.

ABAQUS. 2015. *ABAQUS Documentation*, Providence, RI: Dassault Systèmes, USA.

Ahlbeck, D. R., H. D. Harrison, R. H. Prause, M. R. Johnson. 1976. *Evaluation of Analytical and Experimental Methodologies for the Characterization of Wheel/Rail Loads.* Washington D.C.: Improved Track Structures Research Program, Interim Report. Federal Railroad Administration Office of Research and Development.

Borinder, D. 2014. *Track forces of iron ore wagons—Comparison Between Strain Gauge Based Measurements and Calculated Results.* Stockholm: Master of Science Thesis, University of Stockholm.

Cortis D., M. Bruner, G. Malavasi, S. Rossi, M. Catena, M. Testa. 2017. *Estimation of the wheel-rail lateral contact force through the analysis of the rail web bending strains*. Measurement, Volume 99, March, pp 23-35.

Feng, H. 2011. *3D-models of Railway Track for Dynamic Analysis.* Stockholm, Sweden: Master's Thesis, Division of Highway and Railway Engineering, Royal Institute of Technology.

Kouroussis, G., C. Caucheteur, D. Kinet, G. Alexandrou, O. Verlinden, V. Moeyaert. 2015. *Review of Trackside Monitoring Solutions: From Strain Gages to Optical Fibre Sensors.* Basel, Switzerland: Sensors, Vol. 15, MDPI, pp 20115-20139.

Kudryavtsev, N. N., L. P. Melentyev, A. N. Granovskiy. 1973. *Measurement of Vertical Forces Acting From the Wheels of a Moving Train on the Rails*. Moscow, U.S.S.R: Institute of Railroad Engineering, Herald of the All-Union Scientific-Research Institute of Railroad Transport, No. 6, pp 31-33.

Milkovic´, D., G. Simic´, Ž. Jakovljevic´, J. Tanaskovic´, V. Lučanin. 2013. *Wayside system for wheel–rail contact forces measurements.* Measurement; Journal of the International Measurement Confederation, Vol 46-9, pp 3308-3318.

Mishra, D., E. Tutumluer, H. Bolen. 2014. *Railroad Track Transitions with Multidepth Deflectometers and Strain Gauges.* Washington D.C.: Transportation Research Record: Journal of the Transportation Research Board No. 2448, Transportation Research Board of the National Academies, pp. 105-114.

Moreau A. 1987. *La verification de la sécurité contre le déraillement sur la voie spécialisée de Villeneuve-Saint-Georges*. Revue générale des chemins de fer, pp 25-32. English: Moreau, A. *The security check against the derailment on the specialized track of Villeneuve-Saint-Georges*. General Review of Railways, pp 25-32.

Peterson, L.A., W. H. Freeman, and J. M. Wandrisco. 1971. *Measurement and Analysis of Wheel-Rail Forces.* New York: Premeeting Paper No. 71-WA/RT4, Rail Transportation Division, ASME, August.

Rabbi M. F., D. K. Johnson, D. Mishra, R. Bruzek. 2019. *Effect of Track Configuration and Loading Conditions on Vertical Wheel Load Measurements using the Differential Shear Approach.* Washington, D.C.: Transportation Research Record: Journal of the Transportation Research Board, Transportation Research Board of the National Academies.

Tutumluer, E., D. Mishra, J. H. Hyslip, H. Boler, W. Hou. 2015. *Mitigation of Differential Movement at Railway Transitions for US High Speed Passenger Rail and Joint Passenger/Freight Corridors*. Washington, D.C.: U.S. Department of Transportation, Federal Railroad Administration Office of Railroad Policy and Development, Office of Research and Development.